

Bmi1-Progenitor Cell Ablation Impairs the Angiogenic Response to Myocardial Infarction

Diego Herrero, Susana Cañón, Beatriz Pelacho, María Salvador-Bernáldez, Susana Aguilar, Cristina Pogontke, Rosa María Carmona, Jesús María Salvador, Jose María Perez-Pomares, Ophir David Klein, Felipe Prósper, Luis Jesús Jimenez-Borreguero, Antonio Bernad

Objective—Cardiac progenitor cells reside in the heart in adulthood, although their physiological relevance remains unknown.

Here, we demonstrate that after myocardial infarction, adult Bmi1⁺ (B lymphoma Mo-MLV insertion region 1 homolog [PCGF4]) cardiac cells are a key progenitor-like population in cardiac neovascularization during ventricular remodeling.

Approach and Results—These cells, which have a strong in vivo differentiation bias, are a mixture of endothelial- and mesenchymal-related cells with in vitro spontaneous endothelial cell differentiation capacity. Genetic lineage tracing analysis showed that heart-resident Bmi1⁺ progenitor cells proliferate after acute myocardial infarction and differentiate to generate de novo cardiac vasculature. In a mouse model of induced myocardial infarction, genetic ablation of these cells substantially deteriorated both heart angiogenesis and the ejection fraction, resulting in an ischemic-dilated cardiac phenotype.

Conclusions—These findings imply that endothelial-related Bmi1⁺ progenitor cells are necessary for injury-induced neovascularization in adult mouse heart and highlight these cells as a suitable therapeutic target for preventing dysfunctional left ventricular remodeling after injury. (*Arterioscler Thromb Vasc Biol.* 2018;38:00-00. DOI: 10.1161/ATVBAHA.118.310778.)

Key Words: cell differentiation ■ lymphoma ■ myocardial infarction ■ phenotype ■ ventricular remodeling

Cardiovascular disease is the main cause of morbidity and mortality in the developed world; acute myocardial infarction (AMI), the most prominent cardiac disease in adults, affects millions of people.¹ During AMI, mechanical and chemical stress induce massive loss of cardiomyocytes and cardiac vasculature, followed by a critical revascularization process and formation of a fibrotic scar.² After damage, organized ventricular remodeling is the major determinant of long-term survival.³ To preserve cardiac function after AMI, the mammalian heart develops a hypertrophic response. In some cases, damage evolves to ischemic-dilated phenotype characterized by left ventricular (LV) enlargement, that tends to progress to systolic dysfunction and end-stage disease.⁴ Despite intensive research to identify genetic mutations involved in the development of inherited cardiomyopathies,⁵ only a few studies have focused on the relevance of endogenous adult cell populations in AMI evolution.^{6,7}

Adult cardiac progenitor cells and proliferation of mature cardiac cells are reported to contribute to murine cardiac

cell turnover.^{8,9} Cardiac progenitor cells were described >10 years ago based on c-kit expression.¹⁰ Since then, several adult cardiac progenitor cells have been proposed based on membrane markers (Scal [stem cell antigen-1 (Ly-6A/E)],¹¹ Abcg2,¹² Myh6,¹³ and PDGFR α (platelet-derived growth factor receptor- α)¹⁴) or transcription factors (Isl1,¹⁵ Gli1,⁶ and Bmi1¹⁶), although their contribution to de novo cardiac cell turnover is relatively slow in homeostasis. These cardiac progenitor subsets might represent transient physiological states of a single cell population.

The importance of these adult cardiac cell populations was nonetheless always based on lineage tracing experiments.¹⁷ In contrast to other organs such as intestine,¹⁸ bone marrow (BM),¹⁹ and lung,²⁰ the physiological relevance of cardiac progenitor cells has not been demonstrated functionally by their elimination from the adult heart. Only Gli1⁺ fibroblast progenitor cells have been described as detrimental in ventricular remodeling after AMI.⁶ We previously identified that *Bmi1* is preferentially expressed by a subpopulation of

Received on: January 15, 2018; final version accepted on: June 6, 2018.

From the Department of Immunology and Oncology, National Center for Biotechnology (CNB-CSIC), Madrid, Spain (D.H., S.C., M.S.-B., S.A., R.M.C., J.M.S., A.B.); Center for Applied Medical Research (CIMA) Regenerative Medicine Area, University of Navarra, Pamplona, Spain (B.P., F.P.); IdiSNA, Navarra Institute for Health Research, Pamplona, Spain (B.P., F.P.); Department of Animal Biology, Faculty of Sciences, Instituto de Investigación Biomédica de Málaga (IBIMA) and BIONAND, Centro Andaluz de Nanomedicina y Biotecnología (Junta de Andalucía), Universidad de Málaga, Spain (C.P., J.M.P.-P.); Department of Orofacial Sciences and Program in Craniofacial Biology, University of California San Francisco (O.D.K.); and Cardiovascular Development and Repair Department, National Cardiovascular Research Center (CNIC) and Hospital de La Princesa, Madrid, Spain (L.J.J.-B.).

The online-only Data Supplement is available with this article at <http://atvb.ahajournals.org/lookup/suppl/doi:10.1161/ATVBAHA.118.310778/-/DC1>.

Correspondence to Antonio Bernad, Department of Immunology and Oncology, National Center for Biotechnology (CNB-CSIC), Campus de Cantoblanco de la Universidad Autónoma de Madrid, E-28049 Madrid, Spain. E-mail abernad@cnb.csic.es

© 2018 American Heart Association, Inc.

Arterioscler Thromb Vasc Biol is available at <http://atvb.ahajournals.org>

DOI: 10.1161/ATVBAHA.118.310778

Nonstandard Abbreviations and Acronyms

α -SMA	α -smooth muscle actin
AMI	acute myocardial infarction
BM	bone marrow
Bmi1	B lymphoma Mo-MLV insertion region 1 homolog (PCGF4)
DTA	diphtheria toxin A
GFP	green fluorescent protein
LV	left ventricle
PDGFR α	platelet-derived growth factor receptor- α
RT-qPCR	reverse transcription quantitative PCR
Sca1	stem cell antigen-1 (Ly-6A/E)
Tx	tamoxifen

Sca1⁺ cardiac progenitor cells in murine adult heart (\approx 5% of Sca1⁺ cells), and Sca1⁺Bmi1⁺ cells are able to differentiate to the 3 main cardiac lineages.¹⁶ The physiological relevance of these progenitor cells nonetheless remains undefined. Here, our results indicate that Sca1⁺Bmi1⁺ cardiac cells (hereafter Bmi1⁺ cells) have a mainly endothelial-related phenotype and contribute markedly to de novo cardiac vasculature in post-AMI revascularization. Resident Bmi1⁺ cardiac progenitor cells are necessary for natural ventricular remodeling after AMI; their depletion induces a deficient angiogenic response and increased scar size, leading to an ischemic-dilated cardiac phenotype in mice.

Materials and Methods

The data that support the findings of this study are available from the corresponding author on reasonable request.

Transgenic Mice and Tamoxifen Administration

Transgenic mice were *Bmi1*^{CreERT/+},²¹ *Bmi1*^{GFP/+},²² *Rosa26*^{DTA/+},²³ *Rosa26*^{YFP/+}, *Rosa26*^{Tomato/+} (Ai9), and β -*actin*^{GFP/+} (all from Jackson Laboratory), all on the C57BL/6 background. The full description of transgenic mouse lines and their application in this study can be consulted in Table 1 in the [online-only Data Supplement](#). Tamoxifen (Tx) was dissolved in corn oil (Sigma); mice received Tx (IP) every 24 hours for 3 consecutive days (225 μ g/g body weight daily), or once (7.5 μ g/g body weight) for low Tx induction. Because preliminary analysis showed no differences between male and female mice, all experiments were performed in males and females, as recommended by the US National Institutes of Health.²⁴ Animal studies were approved by the CNB-CSIC Ethics Committee and by the Division of Animal Protection of the Comunidad de Madrid (PA 56/11, PROEX 048/16). All animal procedures conformed to EU Directive 2010/63EU and Recommendation 2007/526/EC about the protection of animals used for experimental and other scientific purposes, enforced in Spanish law under Real Decreto 1201/2005.

AMI and 5-Fluorouracil Treatment

Mice were anesthetized with 4% sevoflurane, intubated, and ventilated with a 50% air:oxygen mixture using a positive-pressure respirator (Minivent 845, Harvard; 160 strokes/min, 250 μ L tidal volume). A left thoracotomy was performed via the fourth intercostal space, and the lungs retracted to expose the heart. After opening the pericardium, we ligated the left anterior descending coronary artery with 7-0 silk suture \approx 2 mm below the edge of the left atrial appendage. Ligation was considered successful when the anterior wall of the LV became pale. The lungs were inflated by

increasing positive end-expiratory pressure, and the thoracotomy site closed in layers with 6-0 suture. Mice were maintained on a 37°C heating pad until recovery and for 2 hours after surgery. Another group of mice underwent sham ligation, with a similar surgical procedure without tightening the suture around the coronary artery.

To induce BM aplasia, 5-fluorouracil (50 mg/kg body weight; Sigma) was administered (intravenously), and hearts were infarcted 4 days after drug treatment.

Human Heart Samples

Human cardiac biopsies were obtained from patients who underwent open-chest surgery, usually for valve replacement. Starting material was obtained from the right atrium appendage, which is routinely removed to place the cannula for extracorporeal circulation. Tissue samples were minced (<1 mm³ pieces) and treated with collagenase type 2 (Worthington Biochemical; 3 cycles, 30 minutes each) to obtain a cell suspension. Cardiomyocytes were removed by centrifugation and filtration using 40 μ m cell strainers. Human c-Kit⁺ and c-Kit⁻ nonmyocyte cells were purified from 3 human myocardial samples by CD45 depletion, followed by c-Kit immunoselection as described,²⁵ and expanded for 2 passages for characterization. Procedures were approved by the hospital ethical committees (Hospital Universitario Gregorio Marañón, Madrid, Spain) with appropriate patient informed consents. All methods were performed in accordance with current guidelines and regulations (RD 9/2014 and Orden SSI/2057/2014, which transpose the European Commission Directive 2012/39/UE). Cells were maintained and expanded in the growth conditions used for the CAREMI clinical trial (EudraCT 2013-001358-81).²⁶

Echocardiography

Mice were anesthetized by isoflurane:oxygen inhalation (1.25:98.75%), and echocardiography performed with a 30-MHz transthoracic echocardiography probe. Images were obtained with the Vevo 2100 micro-ultrasound imaging system (VisualSonics, Toronto, Canada). Measurements of left parasternal long and short axes and M-mode images (left parasternal short axis) were obtained at a heart rate of 500 to 550 bpm. LV end-diastolic diameter (LVEDD), LV end-systolic diameter (LVESD), and wall thickness were measured from M-mode tracings, and the mean of 3 consecutive cardiac cycles is reported. The LV fractional shortening percentage was calculated as ((LVEDD–LVESD)/LVEDD)×100. For image acquisition, we used a combination of volume coil/surface coil to enhance signal-to-noise ratio formed by a 72-mm inner diameter quadrature birdcage TX coil (Rapid Biomedical, Rimpur, Germany) and an actively detuning 30-mm flexible customized surface RX coil (Neos Biotec, Pamplona, Spain). After a tripilot gradient-echo image, a gradient-echo sequence without gating was used to acquire oblique coronal and axial slices. From these images, we determined interventricular septum, LV posterior wall thicknesses, and LV corrected mass; the short-axis M-mode quantification was chosen as most representative. Function was estimated from the ejection fraction and fractional shortening obtained from M-mode views. All procedures were performed blind by 2 echocardiography experts. For ejection fraction measurements, a long- or short-axis view of the heart was selected to obtain an M-mode registration in a line perpendicular to the LV septum and posterior wall at the level of the mitral chordae tendineae.

For echocardiographic analysis of infarct size 5 days after infarction, regional LV function was evaluated in the parasternal long-axis view. The LV wall was subdivided into 13 segments (basal, mid, and apical from the anterior, posterior, lateral and septal walls, as well as the apex). Each segment was scored in a blind manner by an independent evaluator, based on motion and systolic thickening, according to American Society of Echocardiography guidelines (1, normal or hyperkinetic; 2, hypokinetic; 3, akinetic, negligible thickening; 4, dyskinetic, paradoxical systolic motion; and 5, aneurysmal, diastolic deformation).²⁷ The number of dysfunctional segments was quantified, and the total score representing the sum of the score of the 13 individual segments was calculated for each heart.²⁸ At 5 days after

infarction, hearts with a score of ≤ 3 with a mild infarction were discarded from the study.

Histology and Immunohistochemical Analyses

For histological analysis, hearts and small intestines were fixed in 4% paraformaldehyde (PFA; overnight, 4°C), dehydrated and paraffin-embedded for preparation of 10- μm histological sections. Rehydrated slides were stained with Masson trichrome. For immunohistochemistry, hearts and small intestines were fixed in 4% PFA as above and cryopreserved in 30% saccharose, frozen in OCT compound, and sectioned in 8- μm sections on a cryostat. Heart immunohistochemistry and immunocytochemistry have been described.¹⁶ Primary antibodies are shown in Table II in the [online-only Data Supplement](#). A TUNEL assay kit (Roche) was used for histochemical detection of apoptotic cells in heart sections. For histological quantification, at least 30 representative transverse heart or small intestine sections from ventricles and atria were used. Surface areas were quantified by acquiring random images (200 \times) and calculating the number of stained surfaces per total surface, using ImageJ software (US National Institutes of Health). For Bmi1⁺ cell detection at 5-day postlow Tx induction, we measured the number and distance of Bmi1⁺ cells in 2 ventricular serial histological areas (8 μm \times 40 sections) in upper and lower ventricle parts (n=3); we defined a groups of cells as located within a 100 μm radius, considering each histological area as a 3-dimensional structure. Images were captured with a Zeiss LSM 700 or Leica TCS SP5 with fixed settings based on negative controls (isotype controls). Processing, including pseudocolor assignment and changes in brightness, was applied uniformly to the entire image to equalize the appearance of multiple panels in a single figure.

Adult Cardiomyocyte and Nonmyocyte Cell Isolation and Cell Culture

Nonmyocyte cells and cardiomyocytes were obtained by the Langendorff method using retrograde perfusion through the aorta. The heart was removed rapidly and retrograde-perfused under constant pressure (60 mmHg; 37°C, 8 minutes) in Ca²⁺-free buffer (113 mmol/L NaCl, 4.7 mmol/L KCl, 1.2 mmol/L MgSO₄, 5.5 mmol/L glucose, 0.6 mmol/L KH₂PO₄, 0.6 mmol/L Na₂HPO₄, 12 mmol/L NaHCO₃, 10 mmol/L KHCO₃, 10 mmol/L Hepes, 10 mmol/L 2,3-butanedione monoxime, and 30 mmol/L taurine). Digestion was initiated by adding a mixture of recombinant enzymes (0.2 mg/mL Liberase Blendzyme [Roche], 0.14 mg/mL trypsin [ThermoFisher], and 12.5 $\mu\text{mol/L}$ CaCl₂ to the perfusion solution). When the heart became swollen (10 minutes), it was removed and gently teased into small pieces with fine forceps in the enzyme solution. Heart tissue was further dissociated mechanically using 2, 1.5, and 1 mm-diameter pipettes until all large tissue pieces were dispersed. The digestion buffer was neutralized with stopping buffer (10% fetal bovine serum [FBS], 12.5 $\mu\text{mol/L}$ CaCl₂). Cardiomyocytes were pelleted by gravity (7 \times , 30 minutes each), the supernatant contains nonmyocyte cardiac cells.¹⁶

BM Cell Populations

For BM cell analyses, femurs were removed from mice and BM extracted by complete flushing with PBS in sterile conditions. BM populations were defined as hematopoietic progenitors (CD34⁺), pre/pro-B (IgM⁻ B220^{low}), immature B (IgM⁺ B220^{low}), lymphocyte B (IgM⁺ B220^{high}), lymphocyte T-CD4 (TCRb⁺ CD4⁺), lymphocyte T-CD8 (TCRb⁺ CD8⁺), NK-T (TCRb⁺ CD4⁻ CD8⁻), myeloid immature (CD11b^{low} Gr1^{high}), myeloid progenitor+monocytes (CD11b^{low} Gr1^{low}), granulocytes (CD11b^{high} Gr1^{high}), and NK cells (CD11b^{low} Gr1⁻). Antibodies are shown in Table II in the [online-only Data Supplement](#).

In Vitro Cell Culture

Scal⁺ Bmi1⁺ CD31⁻ CD45⁻ and Scal⁺ Bmi1⁺ PDGFR α ⁺ CD45⁻ cells were sorted (BC GALIOS) from nonmyocyte heart fractions and cultured in Iscove's modified Dulbecco's medium (IMDM, Invitrogen) containing 10% fetal bovine serum (Gibco), 100 IU/mL penicillin,

100 mg/mL streptomycin, and 2 mmol/L L-glutamine (all from Invitrogen), 10³ U ESGRO Supplement (Millipore), 10 ng/mL EGF (epidermal growth factor; Sigma), and 20 ng/mL FGF (fibroblast growth factor; Peprotech; 37°C, 3% O₂, 5% CO₂). Primary cardiac endothelial cells (CD31⁺) were obtained by immunomagnetic separation (CD31 MicroBeads, Miltenyi) and cultured in VasculLife VEGF Endothelial Medium Complete Kit (Lifeline Cell Technology; 37°C, 21% O₂, 5% CO₂). Primary cardiac cells were used for the experiments at passage ≤ 9 .

Matrigel Tube Formation Assay

Matrigel tube formation assay was developed and quantified as detailed.²⁹

Cumulative Population Doubling

Cells were passaged as they reached 80% confluence. Cumulative population doubling at each passage was calculated from the cell count with the equation $N_H/N_i = 2^X$, where N_i is inoculum number, N_H is cell harvest number, and X is population doublings. The population doublings were added to yield cumulative population doubling. Replicative senescence is defined as $X < 1$ for 2 weeks.

Flow Cytometry

For flow cytometry analysis, hearts were digested by the Langendorff method and nonmyocyte-enriched fractions analyzed with a Beckman Coulter Moflow XDP cell sorter, and Beckman Coulter GALIOS Analyzer and BD FACSCanto II cytometers. FlowJo vX1 (TreeStar) software was used for data analysis.

Western Blot

For Western blot, cells and tissues were lysed (45 minutes, 4°C) in radioimmunoprecipitation assay buffer (RIPA; Sigma-Aldrich), with the addition of cComplete, EDTA-free Protease Inhibitor Cocktail (Roche). Proteins were quantitated using the Infinite m200 (Tecan). Lysates were size-fractionated by SDS-PAGE, transferred to Hybond ECL nitrocellulose membranes (GE Healthcare), probed with indicated antibodies (Table II in the [online-only Data Supplement](#)), and analyzed by enhanced chemiluminescence (GE Healthcare).

Reverse Transcription Quantitative PCR Analysis

RNA was purified using the Cells-to-CT kit (Ambion, Thermo). Complementary DNA was obtained by reverse transcription with the High Capacity cDNA Reverse Transcription Kit (Applied Biosystems). cDNAs were analyzed by real-time PCR using the Power SYBR Green PCR Master Mix (Applied Biosystems). Amplification, detection, and data analysis were performed with an ABI PRISM 7900HT Sequence Detection System and normalized to *GusB* and *Gapdh* expression. Changes in mRNA expression are noted as x -fold change relative to the control. qPCR primers are listed in Table II in the [online-only Data Supplement](#).

Statistical Analysis

Statistical analyses were performed with GraphPad Prism 6.01. Data were subjected to the Shapiro-Wilk test for normality and F test for equality of variances. For 2 groups, those that passed normality and equal variance tests were analyzed by the Student t test (2-tailed, unpaired) and those that failed normality and equal variance tests were analyzed by nonparametric Mann-Whitney rank-sum test. For multiple groups, data that passed normality and equal variance tests were analyzed by 1-way ANOVA with Tukey post hoc test, and those data that failed normality and equal variance tests were analyzed by the Kruskal-Wallis ANOVA with Dunn multiple comparisons test. To analyze cell distributions, nonparametric 2-sample Kolmogorov-Smirnov test was used. Survival curves were generated by the Kaplan-Meier method and compared using the log-rank test. A value of $P < 0.05$ was considered significant. All replicates considered are biological replicates.

Results

BMI1 Expression Identifies an Endothelial/ Mesenchymal-Related Population of Nonmyocyte Cells in Adult Mouse Heart

We used *Bmi1*^{GFP/+} knock-in mice²² to analyze *Bmi1* expression in heart compared to constitutive GFP (green fluorescent protein) expression in β -actin^{GFP/+} mice. Comparative FACS (fluorescence-activated cell sorting) analyses showed that in

adult heart, *Bmi1* expression was restricted to a subpopulation of nonmyocyte cells (Figure 1A). Whereas the fluorescence intensity in GFP⁺ nonmyocyte cells resembled that of constitutive expression, FACS and immunocytochemistry showed no or very low GFP levels in adult cardiomyocytes (Figure 1B and 1C), as confirmed by reverse transcription quantitative PCR (RT-qPCR; Figure 1D).

To better define the identity of cardiac *Bmi1*⁺ cells, we exhaustively characterized *Bmi1*^{CreERT/+}R26^{Tomato/+} adult heart

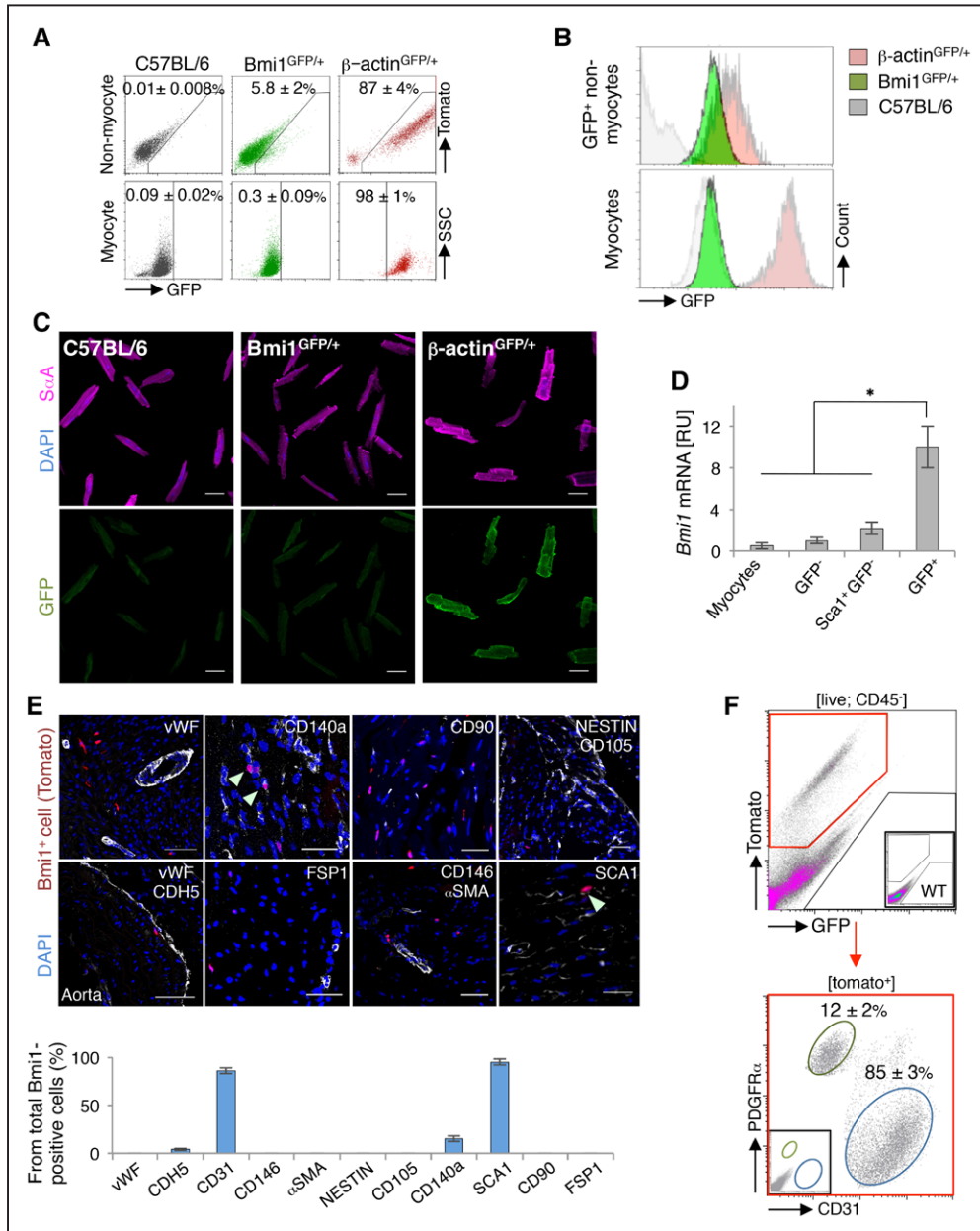


Figure 1. BMI1 (B lymphoma Mo-MLV insertion region 1 homolog [PCGF4]) expression identifies a mixture of endothelial- and mesenchymal-related nonmyocyte cells in the adult heart. **A**, Representative FACS (fluorescence-activated cell sorting) plots of nonmyocyte cells and cardiomyocytes from adult C57BL/6 (grey), *Bmi1*^{GFP/+} (green), and β -actin^{GFP/+} mice (red; n=4). **B**, Histograms of GFP (green fluorescent protein) levels of indicated cardiac cell populations from adult C57BL/6 (grey), *Bmi1*^{GFP/+} (green), and β -actin^{GFP/+} mice (red; n=4). **C**, Representative immunocytochemistry of cardiomyocytes from adult C57BL/6, *Bmi1*^{GFP/+}, and β -actin^{GFP/+} mice. C57BL/6 cardiomyocytes show GFP background. **D**, In vivo *Bmi1* expression of indicated cardiac cell populations from *Bmi1*^{GFP/+} mice (n=4). **P*<0.05; Kruskal-Wallis ANOVA test. Relative units (RU). **E**, **Top**, Immunohistochemical characterization of *Bmi1*⁺ cardiac cells in adult *Bmi1*^{CreERT/+}Rosa26^{Tomato/+} heart cryosections stained with indicated markers at 5-d posttamoxifen (Tx) induction. Arrowheads, double-positive cells. **Bottom**, Immunohistochemical quantification of surface cell marker expression in the *Bmi1*⁺ cardiac cell population (n=3). Bars, 50 μ m. **F**, Representative FACS plot of CD31 and PDGFR α (platelet-derived growth factor receptor- α) surface marker expression in *Bmi1*⁺ cardiac cells from *Bmi1*^{CreERT/+}Rosa26^{Tomato/+} mice, 5-d post-Tx induction (n=4). Data shown as mean \pm SEM. α -SMA indicates α -smooth muscle actin; Sca1, stem cell antigen-1 (Ly-6A/E); vWF, von Willebrand factor; and WT, wild-type.

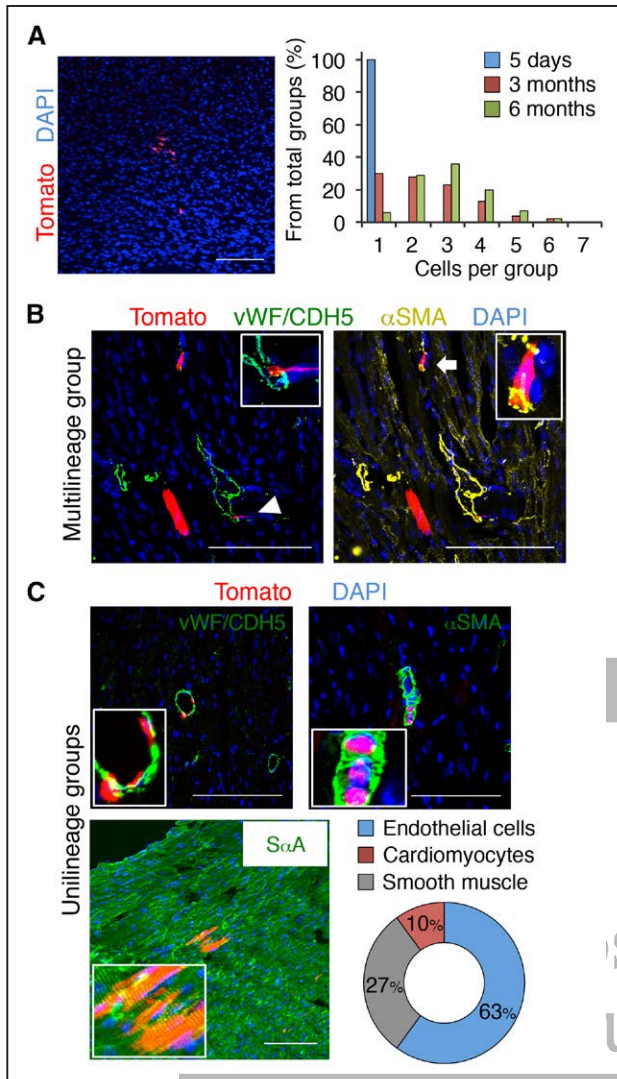


Figure 2. *Bmi1*⁺ cardiac progenitor cells have in vivo differentiation capacity with limited multilineage potential. **A, Left.** Large *Bmi1* (B lymphoma Mo-MLV insertion region 1 homolog [PCGF4]-derived cell group (Tomato) in *Bmi1*^{CreERT/+}*Rosa26*^{Tomato/+} heart, 6-mo postlow tamoxifen (Tx) induction. **Right.** Size quantification of *Bmi1*-derived cell group in cryosections at 5 d, 3- and 6-mo postlow Tx induction (n=3). **B and C.** Representative views of a rare multilineage *Bmi1*-derived cell group (composed of cardiomyocyte, endothelial cell [arrowhead], and smooth muscle [arrow]) (**B**) and more frequent unilineage groups (**C**) in *Bmi1*^{CreERT/+}*Rosa26*^{Tomato/+} hearts, 6-mo postlow Tx induction, with cell type quantification (n=3). Insets, *Bmi1*-derived differentiated cells (×5 magnification). Bars, 100 μm. Data are shown as mean±SEM. α-SMA indicates α-smooth muscle actin; and vWF, von Willebrand factor.

nonspecific CRE activity in the absence of Tx (Figure IVA through IVC in the [online-only Data Supplement](#)). To evaluate system ablation efficiency, we generated the triple transgenic *Bmi1*^{CreERT/+}*R26*^{YFP/DTA} mouse line (Figure 3A). Five days of post-Tx induction, >97% of YFP⁺ cells (2.5±0.4% of total nonmyocyte cells) were eliminated compared with bigenic *Bmi1*^{CreERT/+}*R26*^{YFP/+} control mice (Figure 3A). DTA activity was restricted to nonmyocyte cells, as TUNEL (terminal deoxynucleotidyl transferase dUTP nick end labeling) assay ruled out Tx-related apoptosis in cardiomyocytes at 1- and 5-day post-Tx treatment (Figure IVD in the [online-only Data Supplement](#)). RT-qPCR and Western blot analyses confirmed

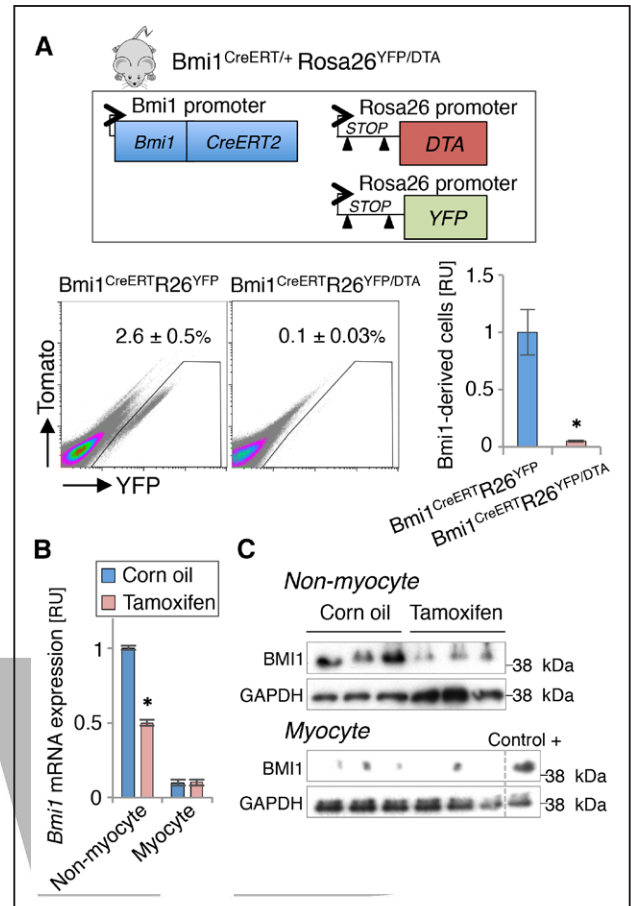


Figure 3. Conditional diphtheria toxin A (DTA) expression induces efficient ablation of adult *Bmi1*⁺ cardiac progenitor cells. **A.** Comparative FACS (fluorescence-activated cell sorting) analyses of *Bmi1*⁺ cardiac progenitor cells (YFP⁺) from bigenic *Bmi1*^{CreERT/+}*Rosa26*^{YFP/+} and trigenic *Bmi1*^{CreERT/+}*Rosa26*^{YFP/DTA} mouse hearts, 5-d posttamoxifen (Tx) induction (n=4). **P*<0.05; Mann-Whitney rank-sum test. **B and C.** Tx treatment-induced downregulation of *Bmi1* expression only in the nonmyocyte fraction in *Bmi1*^{CreERT/+}*Rosa26*^{YFP/DTA} hearts 5-d post-Tx induction, measured by reverse transcription quantitative PCR (RT-qPCR; **B**) and Western blot (**C**; n≥3). Control+: nonmyocyte cells as positive control for *Bmi1* (B lymphoma Mo-MLV insertion region 1 homolog [PCGF4]). **P*<0.05; Mann-Whitney rank-sum test. Data are shown as mean±SEM.

significantly reduced *Bmi1* expression only in the nonmyocyte cell fraction, which indicates successful ablation of *Bmi1*⁺ cardiac progenitor cells after Tx induction (Figure 3B and 3C).

Elimination of *Bmi1*⁺ Progenitor Cells Induces an Ischemic-Dilated Cardiac Phenotype After AMI

With the exception of *Gli1*⁺ fibroblast progenitor cells,⁶ the role of cardiac progenitors after myocardial infarction remains elusive. To test whether *Bmi1*⁺ progenitor cells are necessary after AMI, *Bmi1*^{CreERT/+}*R26*^{DTA/+} mice were randomized and subjected to coronary artery ligation or sham surgery 2-week post-Tx induction. Vehicle-treated [*Bmi1*^{CreERT/+}*R26*^{DTA/+}(CO)] and Tx-treated *R26*^{DTA/+} [*R26*^{DTA/+}(Tx)] mice were used as controls (Figure 4A). Five days post-AMI, echocardiography showed a functional decline in all mice groups regardless of Tx treatment (Figure 4B) and confirmed a similar degree of heart dysfunction (Figure IVE in the [online-only](#)

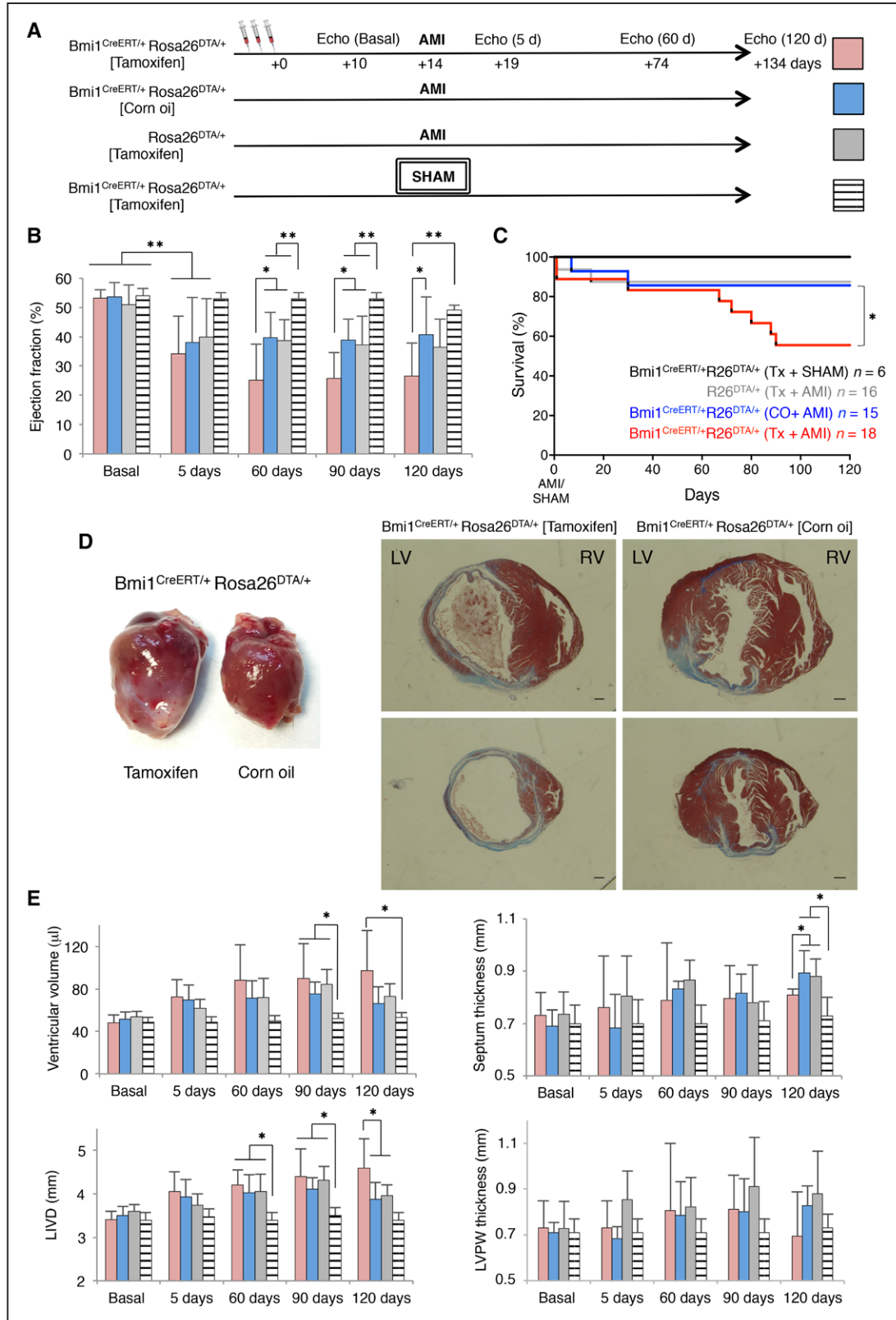


Figure 4. Bmi1⁺ progenitor cells are necessary for natural cardiac remodeling after acute myocardial infarction (AMI). **A**, Timeline echocardiography analyses to evaluate the effects of induced heart injury on the different transgenic mouse lines. Tamoxifen (Tx) induction (d0); AMI (d14). **B**, Trans-thoracic M-mode echocardiography of ejection fraction from infarcted transgenic mice before (basal) and at indicated times after AMI. **P*<0.05, ***P*<0.005; 1-way ANOVA with Tukey post hoc test. **C**, Kaplan-Meier survival curves for the indicated groups of mice. **D**, Gross cardiac phenotype (left) and representative Masson trichrome-stained transverse paraffin sections (right) of Tx- and vehicle-treated Bmi1^{CreERT/+}Rosa26^{DTA/+} hearts, 4 mo after AMI. Bars, 1 mm. **E**, Trans-thoracic M-mode echocardiography of physiological parameters from infarcted transgenic mice before (basal) and at indicated times after AMI. **P*<0.05; 1-way ANOVA with Tukey post hoc test. **B, C, E**, No. of mice (n) per group is indicated in **C**. Data shown as mean±SEM. LVID indicates left internal ventricular diameter; LVPW, left ventricular posterior wall; and RV, right ventricle.

Data Supplement). Two months after damage, echocardiography detected a reduced LV ejection fraction in $Bmi1^{CreERT/+}R26^{DTA/+}$ (Tx) hearts compared with controls (Figure 4B). This cardiac dysfunction was sustained >2 additional months and affected survival of $Bmi1^{+}$ cell-deficient mice (Figure 4C). At this time, histological analysis of $Bmi1^{+}$ cell-deficient hearts confirmed differences in cardiac remodeling compared with infarcted controls. The former presented eccentric cardiac hypertrophy (an ischemic-dilated cardiac phenotype) characterized by LV chamber dilatation, thinning of the interseptal wall, and reduced ejection fraction (Figure 4D and 4E). We found no differences in LV mass as measured by echocardiography or heart/body weight ratio, although we detected a slight increase in myocyte cross-sectional length in $Bmi1^{+}$ cell-deficient hearts (Figure IVF through IVH in the [online-only Data Supplement](#)), possibly linked to an increase in hemodynamic pressure associated with the deficient LV remodeling after AMI.

Prognosis and progression of ischemic damage depend on fibrotic and angiogenic responses after AMI. Deficiencies in these processes affect cardiac remodeling and induce cardiac dysfunction.^{41,42} Quantification of fibrosis in histological sections showed no notable differences between groups (Figure 5A and 5B), although we detected an increase in LV scar size in $Bmi1^{+}$ cell-deficient hearts (Figure 5C). Histological and FACS analyses showed, and RT-qPCR confirmed, that absence of $Bmi1^{+}$ progenitor cells altered the angiogenic response after AMI; mature endothelium was decreased in scar and in remote infarct areas, particularly in small blood vessels (Figure 5D through 5G).

Extracardiac Cell Ablation Does Not Affect Cardiac Function

$Bmi1$ is a marker of various adult stem cell populations,⁴³ and BM is considered the main organ in crosstalk with the heart.⁴⁴ We previously discarded BM origin of $Bmi1^{+}$ cardiac progenitor cells,¹⁶ but it could be possible that $Bmi1$ -cell ablation affected BM-derived cells ($CD45^{+}$). Tx treatment provoked no differences in the percentage of BM populations but induced a nonsignificant decrease in BM cell numbers (Figure VA and VB in the [online-only Data Supplement](#)). In the heart, cardiac resident hematopoietic-derived cells ($CD45^{+}$) were also unaffected (Figure VC and VD in the [online-only Data Supplement](#)). To further confirm the lack of a $Bmi1$ -BM cell role in cardiac dysfunction, we used 5-fluorouracil to induce a decrease in BM cell number, similar to the BM cell ablation after Tx induction in bigenic $Bmi1^{CreERT/+}R26^{DTA/+}$ mice (Figure VE in the [online-only Data Supplement](#)). Echocardiography data showed neither functional nor structural differences in the hearts of PBS- and 5-FU-treated mice 2 months after AMI; results were confirmed in histological sections at 4 months after injury (Figure VF and VG in the [online-only Data Supplement](#)). At this time, BM cellularity and the BM cell populations remained normal in $Bmi1^{+}$ cell-deficient mice (Figure VH and V-I in the [online-only Data Supplement](#)). In addition, despite a decrease of $Lgr5^{+}$ intestinal stem cells 2 days post-Tx treatment, both intestinal stem cell number and crypt-villus architecture in $Bmi1^{CreERT/+}R26^{DTA/+}$ mice 2-week

post-Tx (AMI time point) were comparable to that of vehicle-treated mice (Figure VJ and VK in the [online-only Data Supplement](#)). These results rule out the possibility that extracardiac effects alters adult $Bmi1^{CreERT/+}R26^{DTA/+}$ mouse survival or cardiac function and confirm that resident $Bmi1^{+}$ cardiac progenitor cells are necessary in postischemic angiogenesis.

Conditional Ablation of $Bmi1^{+}$ Cells Does Not Affect Cardiac Function in Steady State

We also monitored the cardiac function of $Bmi1^{+}$ cell-deficient ($Bmi1^{CreERT/+}R26^{DTA/+}$ [Tx-induced]) and control mice ($Bmi1^{CreERT/+}R26^{DTA/+}$ [corn oil vehicle-treated]) for 1 year in homeostasis. In contrast to AMI, we detected no major differences in conventional echocardiography parameters or in cardiac histology in 1-year-old mice (Figure VIA through VID in the [online-only Data Supplement](#)). In accordance, we found no reduction in lifespan in $Bmi1^{+}$ cell-deficient mice (Figure VIE in the [online-only Data Supplement](#)). We analyzed adult cell plasticity⁴⁵ to test whether the absence of phenotype in $Bmi1^{+}$ cell-deficient hearts was at least in part linked to recovery of $Bmi1^{+}$ cardiac cell population in homeostasis. Lineage tracing analysis at 4-month post-Tx of rare surviving $Bmi1^{+}$ progenitor cells in trigenic $Bmi1^{CreERT/+}R26^{YFP/DTA}$ (Tx) mice showed a relative increase in their contribution to cardiac cell progeny compared with bigenic $Bmi1^{CreERT/+}R26^{YFP/+}$ control mice (Figure VIIA through VIIC in the [online-only Data Supplement](#)). In addition, RT-qPCR and Western blot analyses showed no differences in $BMI1$ levels between Tx- and CO-treated mice 4-month postablation in contrast to infarcted mice (Figure VIID through VIIF in the [online-only Data Supplement](#)). The results suggest that, in homeostasis, $Scal^{+}Bmi1^{+}$ cardiac cells are not essential for cardiac function and that the heart could have compensatory mechanisms to replenish $Scal^{+}Bmi1^{+}$ cardiac progenitor cells.

$Bmi1^{+}$ Cardiac Progenitor Cells Are a Source of Endothelial Cells After AMI

We induced lineage tracing in $Bmi1^{CreERT/+}R26^{YFP/+}$ mice to analyze the real contribution of $Bmi1^{+}$ progenitor cells to cardiac progeny after AMI. To exclude the possibility that residual Tx induces CRE activity in $Bmi1^{+}$ cells after injury, hearts were infarcted 2-week post-Tx induction, a period sufficient to ensure its clearance.⁴⁶ We also ruled out an AMI-dependent $BMI1$ upregulation (Figure VIIG in the [online-only Data Supplement](#)). Although we confirmed an increase in $Bmi1$ -derived cardiomyocytes in remote areas at 4 months after AMI⁴⁷ (Figure VIIH in the [online-only Data Supplement](#)), histological and FACS analyses highlighted a relatively large proportion of $Bmi1$ -derived nonmyocyte cells (Figure 6A and 6B). Despite 4 months after damage, we detected a small percentage of cardiac fibroblasts (<8%) derived from $Bmi1^{+}$ progenitor cells (Figure VII-I in the [online-only Data Supplement](#)), we found a striking increase in mature $Bmi1$ -derived endothelial cells (up to 6-fold; Figure 6C). To confirm the endothelial differentiation potential of $Bmi1^{+}$ cardiac cells, we isolated and cultured $Bmi1^{+}CD31^{+}$ and $Bmi1^{+}PDGFR\alpha^{+}$ primary cells from adult $Bmi1^{CreERT/+}R26^{YFP/+}$ mice. Two weeks after cells reached confluence, we observed spontaneous

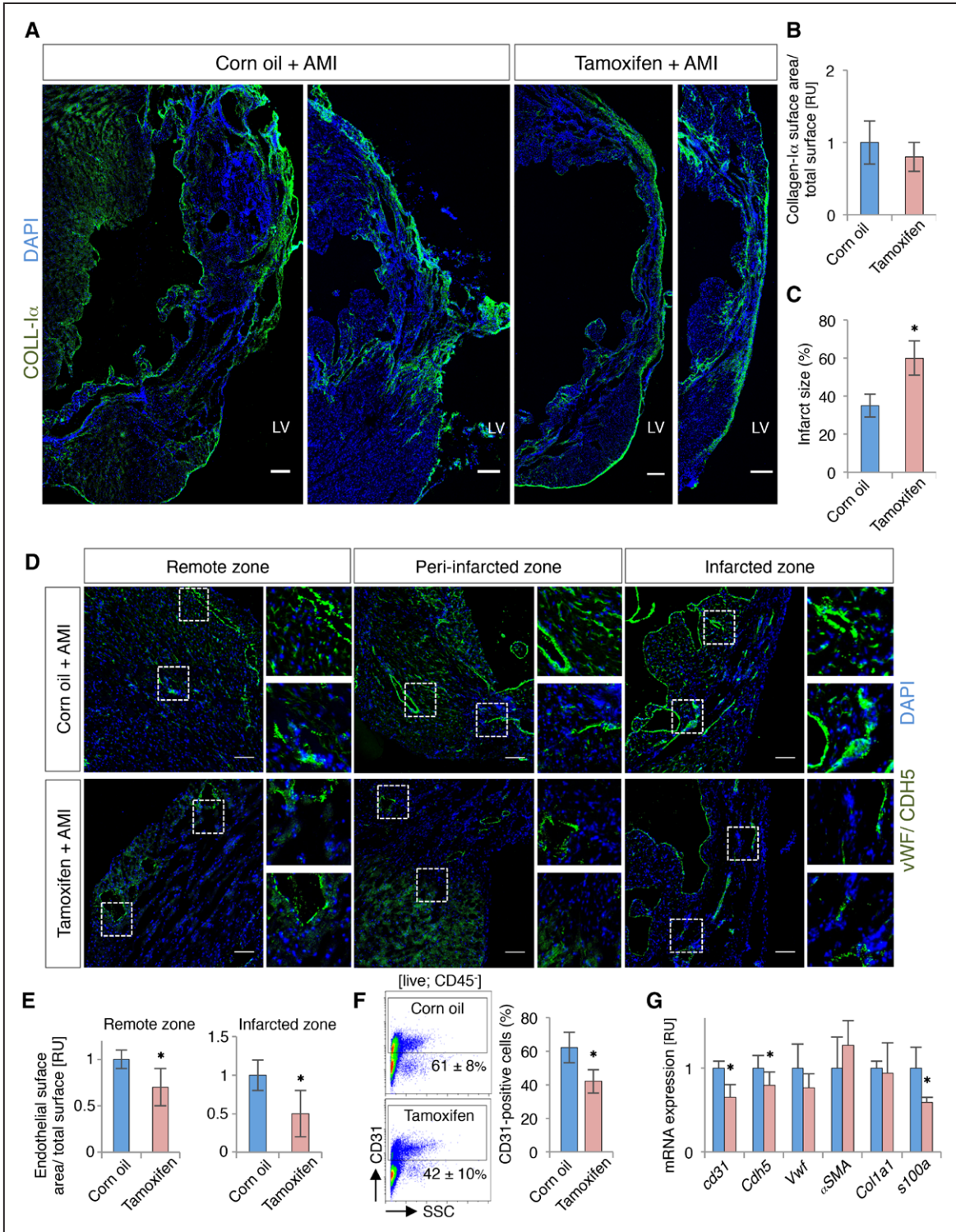


Figure 5. *Bmi1*⁺ cell-deficient hearts show impaired angiogenesis and increased scar size after acute myocardial infarction (AMI). **A**, Representative cryosections of cardiac fibrosis (collagen-1α; coll-1α) from vehicle- and Tamoxifen (Tx)-treated *Bmi1*^{CreERT/+}*Rosa26*^{DTA/+} hearts, 4-mo after AMI. Bars, 100 μm. **B** and **C**, Quantification of collagen-1α deposition (**B**) and left ventricular (LV) scar size (**C**) on cryosections of vehicle- and Tx-treated *Bmi1*^{CreERT/+}*Rosa26*^{DTA/+} mice, 4-mo after AMI (n=5). **D** and **E**, Representative cryosections (**D**) and quantification (**E**) of cardiac vasculature (von Willebrand factor [vWF]/CDH5) from vehicle- and Tx-treated *Bmi1*^{CreERT/+}*Rosa26*^{DTA/+} hearts, 4 mo after AMI (n=5). Bars, 50 μm. **F**, Representative FACS (fluorescence-activated cell sorting) plot (**left**) and quantification (**right**) of CD31⁺ cardiac endothelial cells from vehicle- and Tx-treated *Bmi1*^{CreERT/+}*Rosa26*^{DTA/+} hearts, 2-mo after AMI (n=4). Isotype control in Figure 6D. **G**, *Bmi1*⁺ cell-deficient hearts (red) showed decreased endothelial-related gene expression compared with controls (blue) at 4-mo after AMI, measured by reverse transcription quantitative PCR (RT-qPCR; n=4). Analyses: **P*<0.05; Mann-Whitney rank-sum test. Data are shown as mean±SEM.

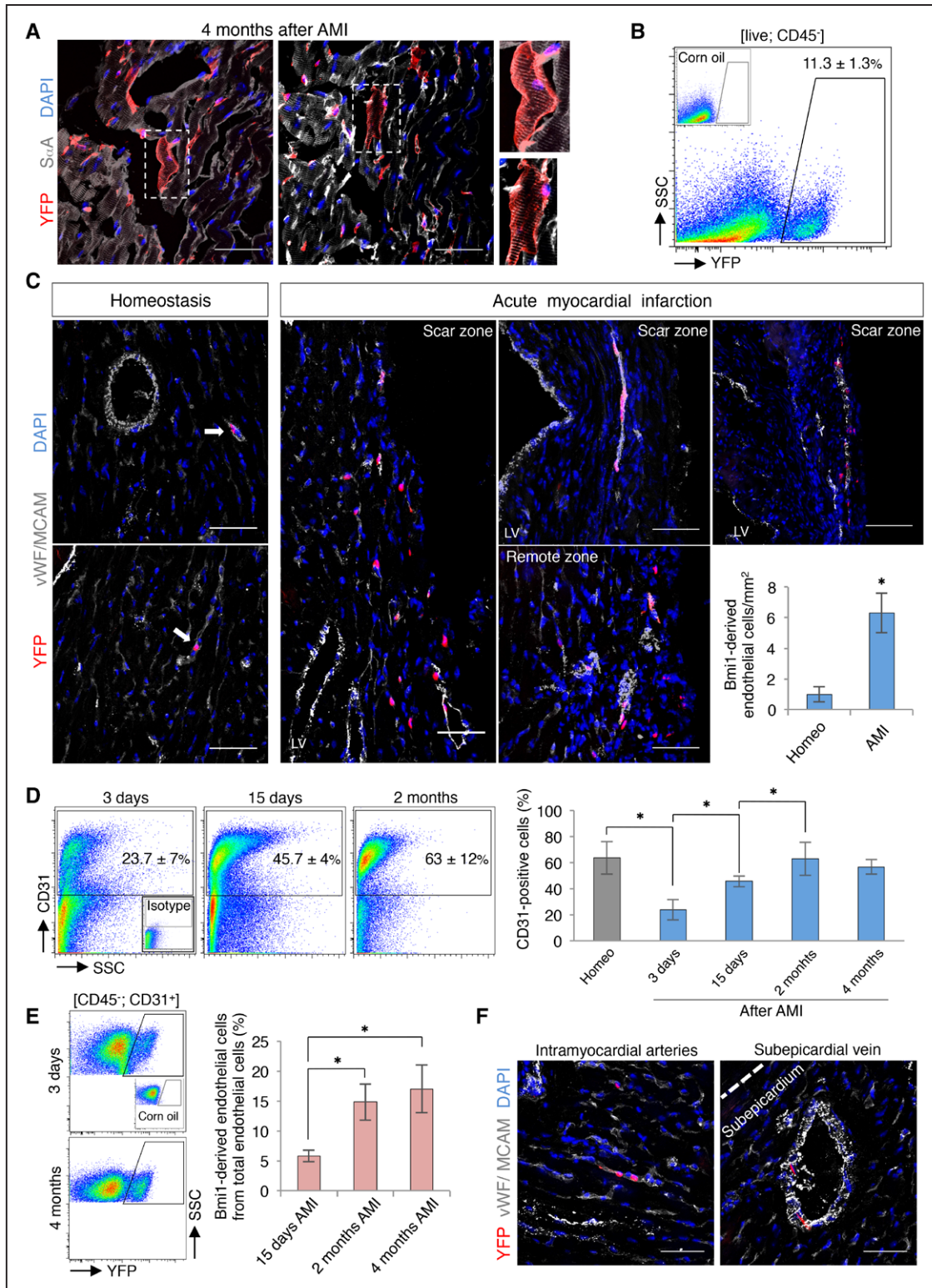


Figure 6. Bmi1⁺ progenitor cells are key contributors to cardiac vasculature after acute myocardial infarction (AMI). **A**, Representative cryosections of Bmi1 (B lymphoma Mo-MLV insertion region 1 homolog [PCGF4])–derived cells (YFP⁺) in remote areas of Bmi1^{CreERT/+}Rosa26^{YFP/+} hearts, 4 mo after AMI. Insets, Bmi1-derived cardiomyocytes (×2 magnification). **B**, FACS (fluorescence-activated cell sorting) analysis of nonmyocyte heart fraction from Bmi1^{CreERT/+}Rosa26^{YFP/+} mice showed a large percentage of Bmi1-derived cells, 4 mo after AMI (n=5). **C**, Representative cryosections and quantification of Bmi1-derived endothelial cells (von Willebrand factor [vWF]/CDH5⁺) in Bmi1^{CreERT/+}Rosa26^{YFP/+} hearts at 4-mo after AMI vs age-matched controls (homeo; n=5). Arrows: Bmi1-derived endothelial cells. *P<0.05; Mann-Whitney rank-sum test. **D**, Representative FACS plots (left) and quantification (right) of cardiac endothelial cells (CD31⁺) in homeostasis and at 3 and 15 d, 2 and 4 mo after AMI in Bmi1^{CreERT/+}Rosa26^{YFP/+} hearts (n≥3). *P<0.05; Kruskal-Wallis ANOVA test. **E**, Representative FACS plots (left) and quantification (right) of Bmi1-derived endothelial cells in Bmi1^{CreERT/+}Rosa26^{YFP/+} hearts during the infarct-induced angiogenic response (n≥4). *P<0.05; Kruskal-Wallis ANOVA test. **F**, Representative views of Bmi1-derived endothelial cells (von Willebrand factor [vWF]/CDH5⁺) in intramyocardial arteries and subepicardial veins of Bmi1^{CreERT/+}Rosa26^{YFP/+} hearts, 4 mo after AMI. Bars, 50 μm. Data shown as mean±SEM. LV indicates left ventricle.

formation of microvascular networks in vitro. Compared with Bmi1⁺PDGFR α ⁺ cells, Bmi1⁺CD31⁺ cardiac cells nonetheless produced a higher percentage and larger-sized endothelial-related structures (Figure VIII in the [online-only Data Supplement](#)).

De novo formation of microvessels is essential for long-term ventricular remodeling after AMI.⁴¹ To evaluate this angiogenic response, we used FACS to quantify in vivo endothelial cell dynamics. Three days after AMI, endothelial cells decreased acutely, probably because of the ischemic process. Revascularization began several days after infarction and was complete at 2 months after AMI (Figure 6D). To analyze the dynamic of Bmi1⁺ cardiac progenitor cells during this revascularization, we also used FACS to trace Bmi1-derived cells from Bmi1^{CreERT/+}R26^{YFP/+} mice. We confirmed a significant contribution of these cells to the angiogenic response, which was especially notable from 2 weeks to 2 months after AMI (Figure 6E). Histological analysis showed Bmi1-derived endothelial cells in infarcted and remote areas, contributing to arterioles in the myocardium and to veins in the subepicardium (Figure 6C and 6F). The results suggest that at 4 months after damage, Bmi1⁺ progenitor cells are a relevant source of cardiac endothelial cells, and contribute up to 20% of total endothelial cells in the infarcted heart.

Discussion

Although knowledge of the effect of gene mutations in cardiac disease development is growing rapidly,⁵ the role of distinct adult cardiac progenitor cell populations after AMI remains poorly understood. Here, we show that after AMI, murine cardiac progenitor-like Sca1⁺Bmi1⁺ cells^{16,47} are necessary for the angiogenic response and that their absence induces ischemic-dilated cardiac phenotype.

Polycomb-related BMI1 protein is necessary for the maintenance of several adult stem cell populations, mainly through its capacity to inhibit senescence-related genes and to regulate mitochondrial function.^{48,49} In-depth analysis of how BMI1 acts has nonetheless allowed description of specific tissue-related functions. In mesenchymal cells, BMI1 inhibits the expression of key chemokines from the senescence-associated secretory phenotype.⁵⁰ In muscle satellite cells, BMI1 enhances progenitor cell protection through metallothionein 1 upregulation.⁵¹ In the heart, recent observations indicate that BMI1 represses a cardiogenic differentiation program,^{52,53} thus identifying cardiac progenitor-like cells.¹⁶ In the majority of tissues, however, high BMI1 expression defines a mixture of progenitor cells and in some cases, Bmi1⁺ cells are not essential for tissue homeostasis.^{54–56} The characteristics and physiological role of Bmi1⁺ progenitor cells in the adult heart remain unexplored.

Our results showed that in murine adult heart, Bmi1⁺ cells are a Sca1⁺ heterogeneous mixture of endothelial- and mesenchymal-related nonmyocyte cells. Expression of the endothelial-related CD31 protein in progenitor cells is not uncommon, as endothelial and progenitor cells are linked in several organs during development, and even in adulthood.^{33,57,58} Proliferation capacity, the mRNA expression profile, and the matrigel angiogenesis assay clearly indicated that cardiac Bmi1⁺ cells are not mature endothelial cells. An in vivo differentiation

assay with a very low dose of Tx showed that, after chase, the majority of Bmi1-derived cell groups were composed of only 1 or 2 mature cell types. The absence of a direct relationship between group size and a number of cardiac cell types might be explained by the more rapid proliferation of endothelial and myofibroblast cells compared with cardiomyocytes,⁵⁹ and by short-term progenitor identity of the majority of Bmi1⁺ cells. Because most studies describe limited multipotency in adult cardiac progenitor cells,^{11,36} it is possible that like other transcription factors, BMI1 expression defines a progenitor-like state of several cell populations in the heart.^{60,61} In the human heart, BMI1 measurement suggests that c-Kit⁺ cardiac stem cells¹⁰ are not the main BMI1 source, whose identification requires additional study.

To evaluate the functional importance of Sca1⁺Bmi1⁺ cells in murine hearts, we used a conditional Cre-mediated cell ablation system.²³ The Rosa26^{DTA} allele allowed high-efficiency removal of Bmi1⁺ cells labeled in the Rosa26^{YFP} reporter allele ($\approx 100\%$ of nonmyocyte cells). CRE deletion efficiency was analogous in both Rosa26 alleles, probably because of the similar size of the deletion fragments and locus accessibility.⁶² One strength of this DTA cellular ablation system is that it allows analysis of cardiac cell dynamics in Bmi1⁺ cell-deficient hearts considering cardiac cell plasticity;⁴⁵ we thus provide a physiological description of the importance of Bmi1⁺ cardiac progenitor cells.

In contrast to our prediction, Bmi1-progenitor cell ablation in homeostasis did not affect cardiac function or mouse lifespan. In homeostasis, BMI1 expression levels were recovered after several months, accompanied by a relative increase in the contribution of Bmi1⁺ cells that escaped ablation to cardiac cell progeny, suggesting cardiac cell plasticity.⁴⁵ The low adult cardiac cell turnover⁵⁹ together with the permissive environment for cell plasticity in homeostasis, and the lack of ischemia-mediated cell activation of Bmi1⁺ cardiac progenitors⁴⁷ may explain the absence of cardiac dysfunction in Bmi1⁺ cell-deficient hearts in homeostasis.

Echocardiography and histological analyses showed that after AMI, nonetheless, Bmi1⁺ cardiac progenitor cells became necessary for correct ventricular remodeling and cardiac function. After infarction, the loss of cardiomyocytes and vasculature, accompanied by formation of a fibrotic scar, induces cardiac remodeling.² In some cases, however, ischemic damage evolves to eccentric hypertrophy (ischemic-dilated phenotype), characterized by an enlarged LV chamber and thinning of the interventricular septum, in which myocytes typically lengthen; these factors lead to reduced cardiac function.⁶³ Histological analysis at 4 months after AMI showed that Bmi1⁺ cell-deficient hearts developed eccentric hypertrophy compared with control hearts. The cellular cause of this pathological remodeling was probably deficient angiogenesis and increased scar size. The absence of increased fibrosis and the fact that disruption of the angiogenic process can increase scar size^{64–66} nonetheless suggest that the cardiac phenotype in Bmi1⁺ cell-deficient hearts is closely linked to impaired injury-induced angiogenesis.

Endothelial cell subpopulations are able to differentiate into cardiomyocytes, pericytes, and fibroblasts in the adult mouse heart.^{30–32} Although endothelial cells make

up the cardiac population with highest cell turnover,⁵⁹ the source of these cells in adult mice is not clear. Several authors describe an important role for BM-derived circulating endothelial progenitor cells.⁶⁷ The mesenchymal-to-endothelial transition is also reported to contribute to substantial numbers of endothelial cells after AMI,⁶⁸ a recent study using several genetic-tracing studies nonetheless challenged these conclusions and suggests that only preexisting endothelial cells and endothelial-related progenitor cells contribute to neovascularization after injury.⁶⁹ Our results showed that Sca1⁺Bmi1⁺ cells are a relevant population during postdamage angiogenesis, and 2 months after AMI contribute up to 20% of total cardiac endothelial cells. Of these Sca1⁺Bmi1⁺ cells, the powerful spontaneous endothelial differentiation capacity of Sca1⁺Bmi1⁺CD31⁺ compared with Sca1⁺Bmi1⁺PDGFR α ⁺ cells in vitro suggests that Sca1⁺Bmi1⁺CD31⁺ cells are the endothelial-related progenitor cell population. The similarity of in vivo cell dynamics and the potential of Sca1⁺Bmi1⁺PDGFR α ⁺ cells to in vitro endothelial differentiation nonetheless stymied our effort to clearly rule out the PDGFR α ⁺ subpopulation.

Depletion of Bmi1⁺ progenitor cells had no effect on cardiac function in homeostasis. Ablation before injury would nonetheless lead to deficient angiogenesis, giving rise to dysfunctional ventricular remodeling and cardiac failure. Our findings suggest that stimulation of endogenous Sca1⁺Bmi1⁺ cardiac progenitor cells in the infarcted myocardium would help counteract the pathological ventricular remodeling by sustaining injury-induced neovascularization.

Acknowledgments

D. Herrero conceived, performed, and designed experiments, developed the project, contributed ideas, and wrote the article. S. Cañón, B. Pelacho, and M. Salvador-Bernaldez performed and designed experiments. C. Pogontke, R.M. Carmona, and S. Aguilar performed experiments. J.M. Perez-Pomares, O.D. Klein, F. Prósper, J.M. Salvador, and L.J. Jimenez-Borreguero cosupervised specific experiments. A. Bernad conceived and developed the project, designed experiments, interpreted results, and wrote the article. All authors read and approved the final article. We thank M.C. Moreno and S. Escudero for the sorting strategy, S. Montalbán and O. Sánchez for assistance with histology, L. Flores and A.V. Alonso for echocardiography analyses, I. Sánchez and L. Domínguez for surgical infarcts, S. Méndez-Ferrer for the Rosa26^{DTA+} mouse line, M. Torres, I. Flores, and N. Fonseca-Balvís for valuable discussion, and C. Mark for editorial assistance.

Sources of Funding

D. Herrero is an FPI predoctoral fellow of the Spanish Ministry of Economy and Competitiveness. This study was supported by grants to A. Bernad from the Ministry of Economy and Competitiveness (MINECO/FEDER; SAF2015-70882-R), Comunidad Autónoma de Madrid (S2011/BMD-2420), Instituto de Salud Carlos III (ISCIII; RETICS-RD12/0018), and the European Commission (HEALTH-2009_242038) to J.M. Perez-Pomares from the MINECO (BFU2015-65783-R) and ISCIII (RD16/0011/0030) to O.D. Klein from the National Institute of Dental and Craniofacial Research (R35-DE026602), and to B. Pelacho from FEDER (ISCIII: PI16/00129 and CPII5/00017).

Disclosures

None.

References

- Benjamin EJ, Blaha MJ, Chiuve SE, et al; American Heart Association Statistics Committee and Stroke Statistics Subcommittee. Heart Disease and Stroke Statistics-2017 Update: a report from the American Heart Association. *Circulation*. 2017;135:e146–e603. doi: 10.1161/CIR.0000000000000485.
- French BA, Kramer CM. Mechanisms of post-infarct left ventricular remodeling. *Drug Discov Today Dis Mech*. 2007;4:185–196. doi: 10.1016/j.ddmec.2007.12.006.
- White HD, Norris RM, Brown MA, Brandt PW, Whitlock RM, Wild CJ. Left ventricular end-systolic volume as the major determinant of survival after recovery from myocardial infarction. *Circulation*. 1987;76:44–51.
- Hershberger RE, Morales A, Siegfried JD. Clinical and genetic issues in dilated cardiomyopathy: a review for genetics professionals. *Genet Med*. 2010;12:655–667. doi: 10.1097/GIM.0b013e3181f2481f.
- Watkins H, Ashrafian H, Redwood C. Inherited cardiomyopathies. *N Engl J Med*. 2011;364:1643–1656. doi: 10.1056/NEJMr0902923.
- Kramann R, Schneider RK, DiRocco DP, Machado F, Fleig S, Bondzie PA, Henderson JM, Ebert BL, Humphreys BD. Perivascular Gli1+ progenitors are key contributors to injury-induced organ fibrosis. *Cell Stem Cell*. 2015;16:51–66. doi: 10.1016/j.stem.2014.11.004.
- Ruiz-Villalba A, Simón AM, Pogontke C, Castillo MI, Abizanda G, Pelacho B, Sánchez-Domínguez R, Segovia JC, Prósper F, Pérez-Pomares JM. Interacting resident epicardium-derived fibroblasts and recruited bone marrow cells form myocardial infarction scar. *J Am Coll Cardiol*. 2015;65:2057–2066. doi: 10.1016/j.jacc.2015.03.520.
- Senyo SE, Steinhauser ML, Pizzimenti CL, Yang VK, Cai L, Wang M, Wu TD, Guerin-Kern JL, Lechene CP, Lee RT. Mammalian heart renewal by pre-existing cardiomyocytes. *Nature*. 2013;493:433–436. doi: 10.1038/nature11682.
- Nakada Y, Canseco DC, Thet S, et al. Hypoxia induces heart regeneration in adult mice. *Nature*. 2017;541:222–227. doi: 10.1038/nature20173.
- Beltrami AP, Barlucchi L, Torella D, Baker M, Limana F, Chimenti S, Kasahara H, Rota M, Musso E, Urbanek K, Leri A, Kajstura J, Nadal-Ginard B, Anversa P. Adult cardiac stem cells are multipotent and support myocardial regeneration. *Cell*. 2003;114:763–776.
- Uchida S, De Gaspari P, Kostin S, Jenniches K, Kilic A, Izumiya Y, Shiojima I, Grosse Kreymborg K, Renz H, Walsh K, Braun T. Sca1-derived cells are a source of myocardial renewal in the murine adult heart. *Stem Cell Reports*. 2013;1:397–410. doi: 10.1016/j.stemcr.2013.09.004.
- Maher TJ, Ren Y, Li Q, Braunlin E, Garry MG, Sorrentino BP, Martin CM. ATP-binding cassette transporter Abcg2 lineage contributes to the cardiac vasculature after oxidative stress. *Am J Physiol Heart Circ Physiol*. 2014;306:H1610–H1618. doi: 10.1152/ajpheart.00638.2013.
- Malliaras K, Ibrahim A, Tseliou E, Liu W, Sun B, Middleton RC, Seinfeld J, Wang L, Sharifi BG, Marbán E. Stimulation of endogenous cardioblasts by exogenous cell therapy after myocardial infarction. *EMBO Mol Med*. 2014;6:760–777. doi: 10.1002/emmm.201303626.
- Noseda M, Harada M, McSweeney S, et al. PDGFR α demarcates the cardiogenic clonogenic Sca1+ stem/progenitor cell in adult murine myocardium. *Nat Commun*. 2015;6:6930. doi: 10.1038/ncomms7930.
- Moretti A, Caron L, Nakano A, Lam JT, Bernshausen A, Chen Y, Qyang Y, Bu L, Sasaki M, Martin-Puig S, Sun Y, Evans SM, Laugwitz KL, Chien KR. Multipotent embryonic isl1+ progenitor cells lead to cardiac, smooth muscle, and endothelial cell diversification. *Cell*. 2006;127:1151–1165. doi: 10.1016/j.cell.2006.10.029.
- Valiente-Alandi I, Albo-Castellanos C, Herrero D, Arza E, Garcia-Gomez M, Segovia JC, Capecchi M, Bernad A. Cardiac Bmi1(+) cells contribute to myocardial renewal in the murine adult heart. *Stem Cell Res Ther*. 2015;6:205. doi: 10.1186/s13287-015-0196-9.
- Santini MP, Forte E, Harvey RP, Kovacic JC. Developmental origin and lineage plasticity of endogenous cardiac stem cells. *Development*. 2016;143:1242–1258. doi: 10.1242/dev.111591.
- Metcalf C, Kljavin NM, Ybarra R, de Sauvage FJ. Lgr5+ stem cells are indispensable for radiation-induced intestinal regeneration. *Cell Stem Cell*. 2014;14:149–159. doi: 10.1016/j.stem.2013.11.008.
- Schoedel KB, Morcos MNF, Zerjatke T, Roeder I, Grinenko T, Voehringer D, Göthert JR, Waskow C, Roers A, Gerbaulet A. The bulk of the hematopoietic stem cell population is dispensable for murine steady-state and stress hematopoiesis. *Blood*. 2016;128:2285–2296. doi: 10.1182/blood-2016-03-706010.
- Dovey JS, Zacharek SJ, Kim CF, Lees JA. Bmi1 is critical for lung tumorigenesis and bronchioalveolar stem cell expansion. *Proc Natl Acad Sci USA*. 2008;105:11857–11862. doi: 10.1073/pnas.0803574105.

21. Sangiorgi E, Capecchi MR. Bmi1 is expressed in vivo in intestinal stem cells. *Nat Genet.* 2008;40:915–920. doi: 10.1038/ng.165.
22. Hosen N, Yamane T, Muijijens M, Pham K, Clarke MF, Weissman IL. Bmi-1-green fluorescent protein-knock-in mice reveal the dynamic regulation of Bmi-1 expression in normal and leukemic hematopoietic cells. *Stem Cells.* 2007;25:1635–1644. doi: 10.1634/stemcells.2006-0229.
23. Brockschneider D, Pechmann Y, Sonnenberg-Riethmacher E, Riethmacher D. An improved mouse line for Cre-induced cell ablation due to diphtheria toxin A, expressed from the Rosa26 locus. *Genesis.* 2006;44:322–327. doi: 10.1002/dvg.20218.
24. Robinet P, Milewicz DM, Cassis LA, Leeper NJ, Lu HS, Smith JD. Consideration of sex differences in design and reporting of experimental arterial pathology studies-statement from ATVB Council. *Arterioscler Thromb Vasc Biol.* 2018;38:292–303. doi: 10.1161/ATVBAHA.117.309524.
25. Lauden L, Boukouaci W, Borlado LR, López IP, Sepúlveda P, Tamouza R, Charron D, Al-Daccak R. Allogenicity of human cardiac stem/progenitor cells orchestrated by programmed death ligand 1. *Circ Res.* 2013;112:451–464. doi: 10.1161/CIRCRESAHA.112.276501.
26. Torán JL, Aguilar S, López JA, Torroja C, Quintana JA, Santiago C, Abad JL, Gomes-Alves P, Gonzalez A, Bernal JA, Jiménez-Borreguero LJ, Alves PM, R-Borlado L, Vázquez J, Bernad A. CXCL6 is an important paracrine factor in the pro-angiogenic human cardiac progenitor-like cell secretome. *Sci Rep.* 2017;7:12490. doi: 10.1038/s41598-017-11976-6.
27. Lang RM, Bierig M, Devereux RB, Flachskampf FA, Foster E, Pellikka PA, Picard MH, Roman MJ, Seward J, Shanewise JS, Solomon SD, Spencer KT, Sutton MS, Stewart WJ; Chamber Quantification Writing Group; American Society of Echocardiography's Guidelines and Standards Committee; European Association of Echocardiography. Recommendations for chamber quantification: a report from the American Society of Echocardiography's Guidelines and Standards Committee and the Chamber Quantification Writing Group, developed in conjunction with the European Association of Echocardiography, a branch of the European Society of Cardiology. *J Am Soc Echocardiogr.* 2005;18:1440–1463. doi: 10.1016/j.echo.2005.10.005.
28. López-Olañeta MM, Villalba M, Gómez-Salineró JM, Jiménez-Borreguero LJ, Breckenridge R, Ortiz-Sánchez P, García-Pavía P, Ibáñez B, Lara-Pezzi E. Induction of the calcineurin variant CnAβ1 after myocardial infarction reduces post-infarction ventricular remodeling by promoting infarct vascularization. *Cardiovasc Res.* 2014;102:396–406. doi: 10.1093/cvr/cvu068.
29. DeCicco-Skinner KL, Henry GH, Cataisson C, Tabib T, Gwilliam JC, Watson NJ, Bullwinkle EM, Falkenburg L, O'Neill RC, Morin A, Wiest JS. Endothelial cell tube formation assay for the in vitro study of angiogenesis. *J Vis Exp.* 2014:e51312.
30. Fiore BA, Heimfeld JD, Paik DT, Hatzopoulos AK. Endothelial cells contribute to generation of adult ventricular myocytes during cardiac homeostasis. *Cell Rep.* 2014;8:229–241. doi: 10.1016/j.celrep.2014.06.004.
31. Chen Q, Zhang H, Liu Y, Adams S, Eilken H, Stehling M, Corada M, Dejana E, Zhou B, Adams RH. Endothelial cells are progenitors of cardiac pericytes and vascular smooth muscle cells. *Nat Commun.* 2016;7:12422. doi: 10.1038/ncomms12422.
32. Zeisberg EM, Tarnavski O, Zeisberg M, Dorfman AL, McMullen JR, Gustafsson E, Chandraker A, Yuan X, Pu WT, Roberts AB, Neilson EG, Sayegh MH, Izumo S, Kalluri R. Endothelial-to-mesenchymal transition contributes to cardiac fibrosis. *Nat Med.* 2007;13:952–961. doi: 10.1038/nm1613.
33. Padrón-Barthe L, Temiño S, Villa del Campo C, Carramolino L, Isern J, Torres M. Clonal analysis identifies homogenic endothelium as the source of the blood-endothelial common lineage in the mouse embryo. *Blood.* 2014;124:2523–2532. doi: 10.1182/blood-2013-12-545939.
34. Ito K, Turcotte R, Cui J, et al. Self-renewal of a purified Tie2⁺ hematopoietic stem cell population relies on mitochondrial clearance. *Science.* 2016;354:1156–1160. doi: 10.1126/science.aaf5530.
35. Sultana N, Zhang L, Yan J, Chen J, Cai W, Razaque S, Jeong D, Sheng W, Bu L, Xu M, Huang GY, Hajjar RJ, Zhou B, Moon A, Cai CL. Resident c-kit(+) cells in the heart are not cardiac stem cells. *Nat Commun.* 2015;6:8701. doi: 10.1038/ncomms9701.
36. van Berlo JH, Kanisicak O, Maillat M, Vagnozzi RJ, Karch J, Lin SC, Middleton RC, Marbán E, Molkentin JD. c-kit+ cells minimally contribute cardiomyocytes to the heart. *Nature.* 2014;509:337–341. doi: 10.1038/nature13309.
37. Anversa P, Kajstura J, Rota M, Leri A. Regenerating new heart with stem cells. *J Clin Invest.* 2013;123:62–70. doi: 10.1172/JCI63068.
38. Birbrair A, Borges IDT, Gilson Sena IF, Almeida GG, da Silva Meirelles L, Gonçalves R, Mintz A, Delbono O. How plastic are pericytes? *Stem Cells Dev.* 2017;26:1013–1019. doi: 10.1089/scd.2017.0044.
39. Guimarães-Camboa N, Cattaneo P, Sun Y, Moore-Morris T, Gu Y, Dalton ND, Rockenstein E, Masliah E, Peterson KL, Stallcup WB, Chen J, Evans SM. Pericytes of multiple organs do not behave as mesenchymal stem cells in vivo. *Cell Stem Cell.* 2017;20:345.e5–359.e5. doi: 10.1016/j.stem.2016.12.006.
40. Drummond-Barbosa D. Stem cells, their niches and the systemic environment: an aging network. *Genetics.* 2008;180:1787–1797. doi: 10.1534/genetics.108.098244.
41. Cochain C, Channon KM, Silvestre JS. Angiogenesis in the infarcted myocardium. *Antioxid Redox Signal.* 2013;18:1100–1113. doi: 10.1089/ars.2012.4849.
42. Talman V, Ruskoaho H. Cardiac fibrosis in myocardial infarction-from repair and remodeling to regeneration. *Cell Tissue Res.* 2016;365:563–581. doi: 10.1007/s00441-016-2431-9.
43. Bhattacharya R, Mustafi SB, Street M, Dey A, Dwivedi SK. Bmi-1: at the crossroads of physiological and pathological biology. *Genes Dis.* 2015;2:225–239. doi: 10.1016/j.gendis.2015.04.001.
44. Balmer GM, Bollini S, Dubé KN, Martínez-Barbera JP, Williams O, Riley PR. Dynamic hematopoietic cell contribution to the developing and adult epicardium. *Nat Commun.* 2014;5:4054. doi: 10.1038/ncomms5054.
45. Das S, Red-Horse K. Cellular plasticity in cardiovascular development and disease. *Dev Dyn.* 2017;246:328–335. doi: 10.1002/dvdy.24486.
46. Robinson SP, Langan-Fahey SM, Johnson DA, Jordan VC. Metabolites, pharmacodynamics, and pharmacokinetics of tamoxifen in rats and mice compared to the breast cancer patient. *Drug Metab Dispos.* 1991;19:36–43.
47. Valiente-Alandi I, Albo-Castellanos C, Herrero D, Sanchez I, Bernad A. Bmi1 (+) cardiac progenitor cells contribute to myocardial repair following acute injury. *Stem Cell Res Ther.* 2016;7:100. doi: 10.1186/s13287-016-0355-7.
48. Jacobs JJ, Kieboom K, Marino S, DePinho RA, van Lohuizen M. The oncogene and Polycomb-group gene Bmi-1 regulates cell proliferation and senescence through the Ink4a locus. *Nature.* 1999;397:164–168. doi: 10.1038/16476.
49. Banerjee Mustafi S, Aznar N, Dwivedi SK, Chakraborty PK, Basak R, Mukherjee P, Ghosh P, Bhattacharya R. Mitochondrial BMI1 maintains bioenergetic homeostasis in cells. *FASEB J.* 2016;30:4042–4055. doi: 10.1096/fj.201600321R.
50. Jin HJ, Lee HJ, Heo J, Lim J, Kim M, Kim MK, Nam HY, Hong GH, Cho YS, Choi SJ, Kim IG, Shin DM, Kim SW. Senescence-associated MCP-1 secretion is dependent on a decline in BMI1 in human mesenchymal stromal cells. *Antioxid Redox Signal.* 2016;24:471–485. doi: 10.1089/ars.2015.6359.
51. Di Foggia V, Zhang X, Licastro D, Gerli MF, Phadke R, Muntoni F, Mourikis P, Tajbakhsh S, Ellis M, Greaves LC, Taylor RW, Cossu G, Robson LG, Marino S. Bmi1 enhances skeletal muscle regeneration through MT1-mediated oxidative stress protection in a mouse model of dystrophinopathy. *J Exp Med.* 2014;211:2617–2633. doi: 10.1084/jem.20140317.
52. Zhou Y, Wang L, Vaseghi HR, Liu Z, Lu R, Alimohamadi S, Yin C, Fu JD, Wang GG, Liu J, Qian L. Bmi1 is a key epigenetic barrier to direct cardiac reprogramming. *Cell Stem Cell.* 2016;18:382–395. doi: 10.1016/j.stem.2016.02.003.
53. Herrero D, Tomé M, Cañón S, Cruz FM, Carmona RM, Fuster E, Roche E, Bernad A. Redox-dependent BMI1 activity drives in vivo adult cardiac progenitor cell differentiation. *Cell Death Differ.* 2018;25:807–820. doi: 10.1038/s41418-017-0022-2.
54. Yan KS, Chia LA, Li X, Ootani A, Su J, Lee JY, Su N, Luo Y, Heilshorn SC, Amieva MR, Sangiorgi E, Capecchi MR, Kuo CJ. The intestinal stem cell markers Bmi1 and Lgr5 identify two functionally distinct populations. *Proc Natl Acad Sci USA.* 2012;109:466–471. doi: 10.1073/pnas.1118857109.
55. Komai Y, Tanaka T, Tokuyama Y, Yanai H, Ohe S, Omachi T, Atsumi N, Yoshida N, Kumano K, Hisha H, Matsuda T, Ueno H. Bmi1 expression in long-term germ stem cells. *Sci Rep.* 2014;4:6175. doi: 10.1038/srep06175.
56. Biehs B, Hu JK, Strauli NB, Sangiorgi E, Jung H, Heber RP, Ho S, Goodwin AF, Dasen JS, Capecchi MR, Klein OD. BMI1 represses Ink4a/Arf and Hox genes to regulate stem cells in the rodent incisor. *Nat Cell Biol.* 2013;15:846–852. doi: 10.1038/ncb2766.
57. Shen Q, Goderie SK, Jin L, Karanth N, Sun Y, Abramova N, Vincent P, Pumiglia K, Temple S. Endothelial cells stimulate self-renewal and expand neurogenesis of neural stem cells. *Science.* 2004;304:1338–1340. doi: 10.1126/science.1095505.

58. Kunisaki Y, Bruns I, Scheiermann C, Ahmed J, Pinho S, Zhang D, Mizoguchi T, Wei Q, Lucas D, Ito K, Mar JC, Bergman A, Frenette PS. Arteriolar niches maintain haematopoietic stem cell quiescence. *Nature*. 2013;502:637–643. doi: 10.1038/nature12612.
59. Bergmann O, Zdunek S, Felker A, et al. Dynamics of cell generation and turnover in the human heart. *Cell*. 2015;161:1566–1575. doi: 10.1016/j.cell.2015.05.026.
60. Bunting KD. ABC transporters as phenotypic markers and functional regulators of stem cells. *Stem Cells*. 2002;20:11–20. doi: 10.1634/stemcells.20-3-274.
61. Sarkar A, Hochedlinger K. The sox family of transcription factors: versatile regulators of stem and progenitor cell fate. *Cell Stem Cell*. 2013;12:15–30. doi: 10.1016/j.stem.2012.12.007.
62. Liu J, Willet SG, Bankaitis ED, Xu Y, Wright CV, Gu G. Non-parallel recombination limits cre-loxp-based reporters as precise indicators of conditional genetic manipulation. *Genesis*. 2013;51:436–442.
63. McNally EM, Golbus JR, Puckelwartz MJ. Genetic mutations and mechanisms in dilated cardiomyopathy. *J Clin Invest*. 2013;123:19–26. doi: 10.1172/JCI162862.
64. Wang J, Hoshijima M, Lam J, Zhou Z, Jokiel A, Dalton ND, Hultenby K, Ruiz-Lozano P, Ross J Jr, Tryggvason K, Chien KR. Cardiomyopathy associated with microcirculation dysfunction in laminin alpha4 chain-deficient mice. *J Biol Chem*. 2006;281:213–220. doi: 10.1074/jbc.M505061200.
65. Shiojima I, Sato K, Izumiya Y, Schiekofer S, Ito M, Liao R, Colucci WS, Walsh K. Disruption of coordinated cardiac hypertrophy and angiogenesis contributes to the transition to heart failure. *J Clin Invest*. 2005;115:2108–2118. doi: 10.1172/JCI24682.
66. Kivelä R, Bry M, Robciuc MR, et al. VEGF-B-induced vascular growth leads to metabolic reprogramming and ischemia resistance in the heart. *EMBO Mol Med*. 2014;6:307–321. doi: 10.1002/emmm.201303147.
67. Asahara T, Murohara T, Sullivan A, Silver M, van der Zee R, Li T, Witzenbichler B, Schatteman G, Isner JM. Isolation of putative progenitor endothelial cells for angiogenesis. *Science*. 1997;275:964–967.
68. Ubil E, Duan J, Pillai IC, Rosa-Garrido M, Wu Y, Bargiacchi F, Lu Y, Stanboulou S, Huang J, Rojas M, Vondriska TM, Stefani E, Deb A. Mesenchymal-endothelial transition contributes to cardiac neovascularization. *Nature*. 2014;514:585–590. doi: 10.1038/nature13839.
69. He L, Huang X, Kanisicak O, et al. Preexisting endothelial cells mediate cardiac neovascularization after injury. *J Clin Invest*. 2017;127:2968–2981. doi: 10.1172/JCI93868.

Highlights

- Sca1⁺Bmi1⁺ progenitor cells are dispensable for cardiac homeostasis in adult mice.
- Sca1⁺Bmi1⁺ progenitor cells are important for infarct-induced neovascularization.
- Sca1⁺Bmi1⁺CD31⁺ progenitor subpopulation is highly prone to endothelial cell generation.



ATVB

Arteriosclerosis, Thrombosis, and Vascular Biology

FIRST PROOF ONLY

Arteriosclerosis, Thrombosis, and Vascular Biology



JOURNAL OF THE AMERICAN HEART ASSOCIATION

Bmi1-Progenitor Cell Ablation Impairs the Angiogenic Response to Myocardial Infarction

Diego Herrero, Susana Cañón, Beatriz Pelacho, María Salvador-Bernáldez, Susana Aguilar, Cristina Pogontke, Rosa María Carmona, Jesús María Salvador, Jose María Perez-Pomares, Ophir David Klein, Felipe Prósper, Luis Jesús Jimenez-Borreguero and Antonio Bernad

Arterioscler Thromb Vasc Biol. published online June 21, 2018;

Arteriosclerosis, Thrombosis, and Vascular Biology is published by the American Heart Association, 7272 Greenville Avenue, Dallas, TX 75231

Copyright © 2018 American Heart Association, Inc. All rights reserved.

Print ISSN: 1079-5642. Online ISSN: 1524-4636

The online version of this article, along with updated information and services, is located on the World Wide Web at:

<http://atvb.ahajournals.org/content/early/2018/06/20/ATVBAHA.118.310778>

Data Supplement (unedited) at:

<http://atvb.ahajournals.org/content/suppl/2018/06/19/ATVBAHA.118.310778.DC1>

Permissions: Requests for permissions to reproduce figures, tables, or portions of articles originally published in *Arteriosclerosis, Thrombosis, and Vascular Biology* can be obtained via RightsLink, a service of the Copyright Clearance Center, not the Editorial Office. Once the online version of the published article for which permission is being requested is located, click Request Permissions in the middle column of the Web page under Services. Further information about this process is available in the [Permissions and Rights Question and Answer](#) document.

Reprints: Information about reprints can be found online at:

<http://www.lww.com/reprints>

Subscriptions: Information about subscribing to *Arteriosclerosis, Thrombosis, and Vascular Biology* is online at:

<http://atvb.ahajournals.org/subscriptions/>

SUPPLEMENTAL MATERIAL

Bmi1-progenitor cell ablation impairs the angiogenic response to myocardial infarction

Diego Herrero¹, Susana Cañón¹, Beatriz Pelacho², María Salvador-Bernáldez¹, Susana Aguilar¹, Cristina Pogontke³, Rosa María Carmona¹, Jesús María Salvador¹, Jose María Perez-Pomares³, Ophir David Klein⁴, Felipe Prósper², Luis Jesús Jimenez-Borreguero⁵, Antonio Bernad^{1*}

¹Department of Immunology and Oncology, National Center for Biotechnology (CNB-CSIC), 28049 Madrid, Spain

²Center for Applied Medical Research (CIMA) Cell Therapy Area, IdiSNA, Universidad de Navarra, 31080 Pamplona, Spain

³Department of Animal Biology, Faculty of Sciences, Instituto de Investigación Biomédica de Málaga (IBIMA), University of Málaga, 29071 Malaga & BIONAND, Centro Andaluz de Nanomedicina y Biotecnología (Junta de Andalucía, Universidad de Málaga), 29590 Málaga, Spain

⁴Department of Orofacial Sciences and Program in Craniofacial Biology, University of California San Francisco, San Francisco, CA 94143, USA

⁵Cardiovascular Development and Repair Department, National Cardiovascular Research Center (CNIC), 28029 Madrid & Hospital de la Princesa, 28006, Madrid, Spain

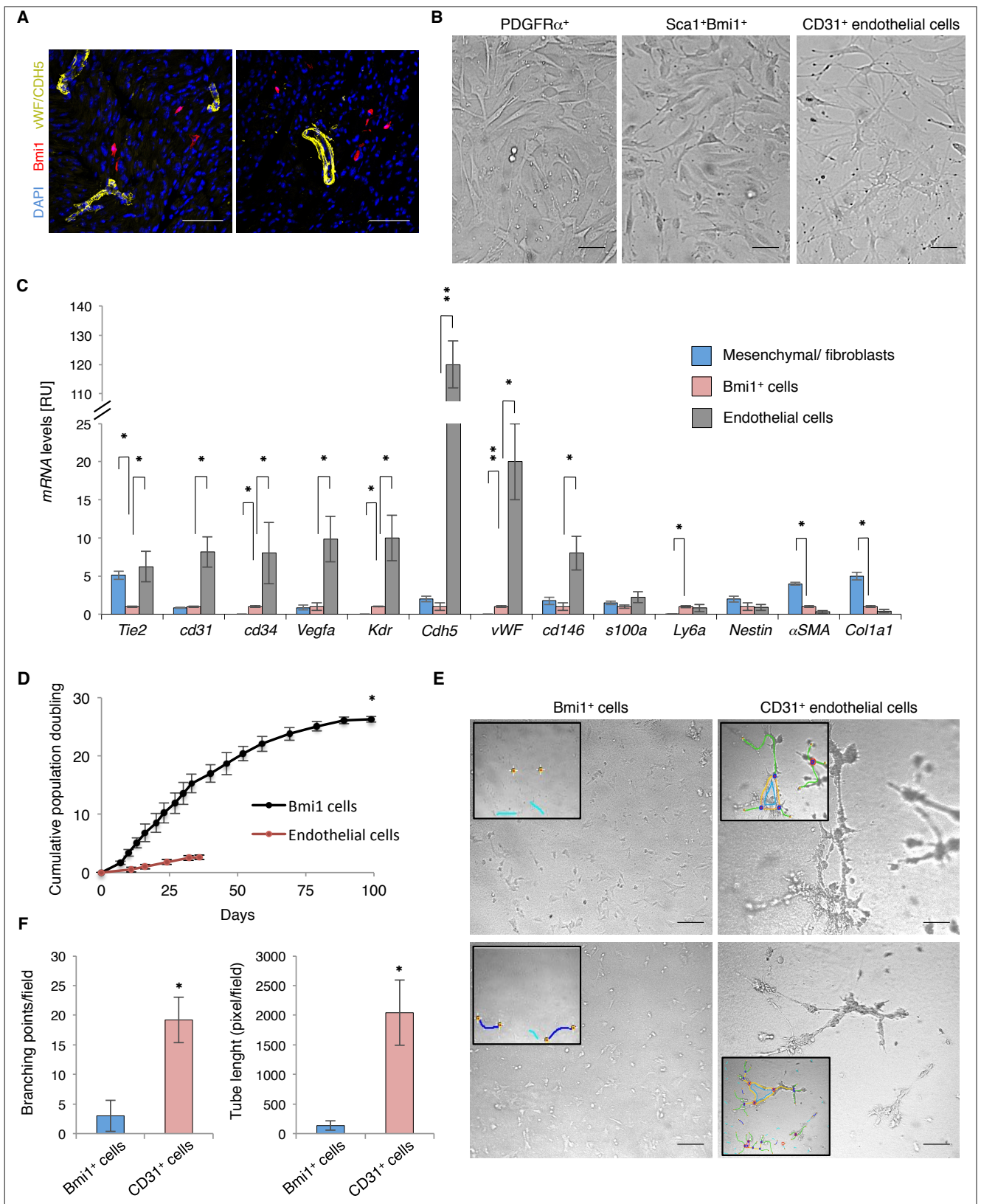


Figure 1. Bmi1⁺ cells are not a subpopulation of mature endothelial cells. **A**, vWF/CDH5-immunohistochemistry of heart cryosections of Bmi1^{CreERT/+}Rosa26^{YFP/+} mice, 5 days post-Tx. **B**, Representative phase contrast images for the three indicated primary cardiac cell populations. **C**, RT-qPCR analysis of endothelial- and fibroblast-related mRNA gene expression in indicated primary cardiac cells (passage 4) from Bmi1^{CreERT/+}Rosa26^{YFP/+} mice ($n = 4$). * $p < 0.05$, ** $p < 0.005$; Kruskal-Wallis ANOVA test. **D**, Cumulative population doubling of primary Bmi1⁺ and endothelial cells isolated from Bmi1^{CreERT/+}Rosa26^{YFP/+} mice ($n = 3$). * $p < 0.05$; Mann-Whitney rank sum test. **E** and **F**, Representative images of tubular network formation (**E**) and quantification (**F**) in a matrigel assay for Bmi1⁺ and endothelial primary cardiac cells. *Insets*, tubular network quantification. * $p < 0.05$; Mann-Whitney rank sum test. Bars, 50 μ m. Data shown as mean \pm SEM.

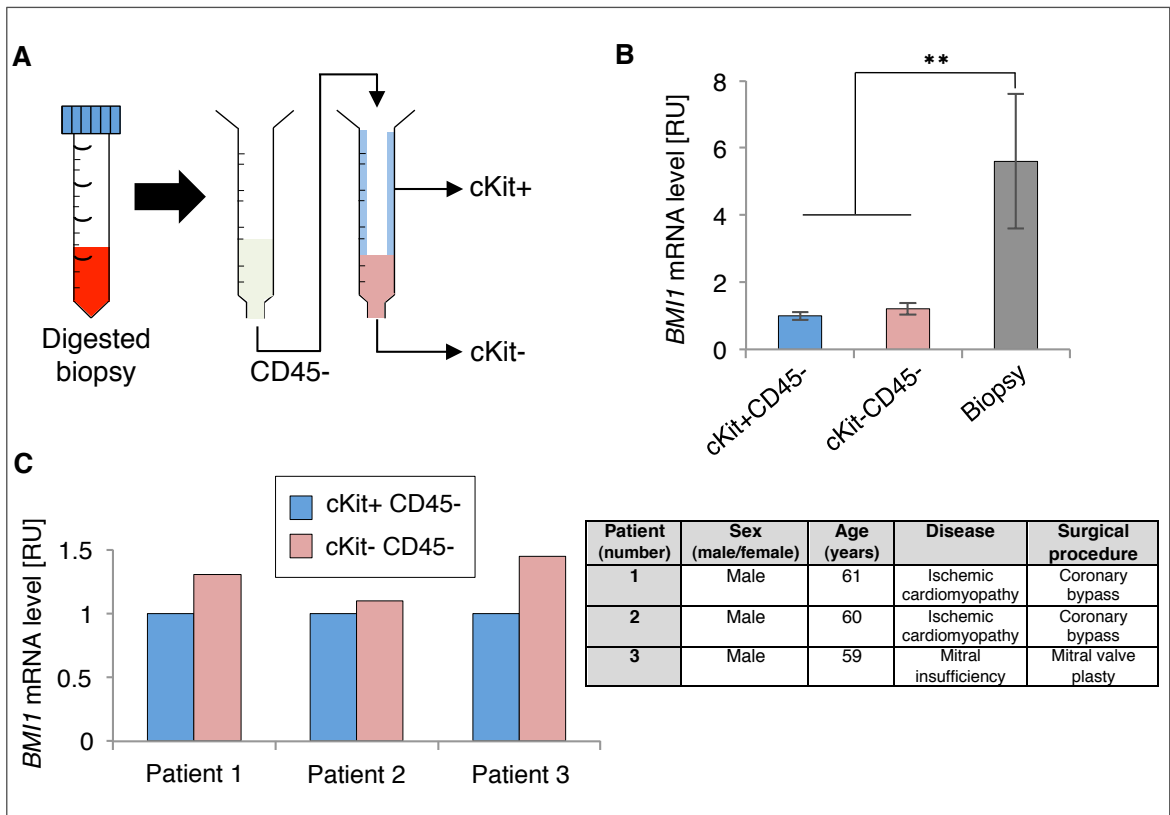


Figure II. c-Kit⁺ cardiac stem cells are not the main source of *BMI1* in human heart. **A**, Cardiac cell isolation from human heart biopsies. After enzymatic digestion to single cells, hematopoietic-derived cells (CD45⁺) were depleted from the cell suspension; c-Kit⁺ and c-Kit⁻ cells were sorted magnetically. **B**, *BMI1* mRNA level in fresh biopsies ($n = 5$) compared to *in vitro*-cultured primary (passage 2) c-Kit⁺CD45⁻ ($n = 3$) and c-Kit⁻CD45⁻ ($n = 3$) cells. ** $p < 0.005$; Kruskal-Wallis ANOVA test. **C**, Individual *BMI1* expression in c-Kit⁺ and c-Kit⁻ cardiac cells isolated in parallel from the same donor ($n = 3$). Experimental triplicates. n.s.; Mann-Whitney rank sum test. Data shown as mean \pm SEM.

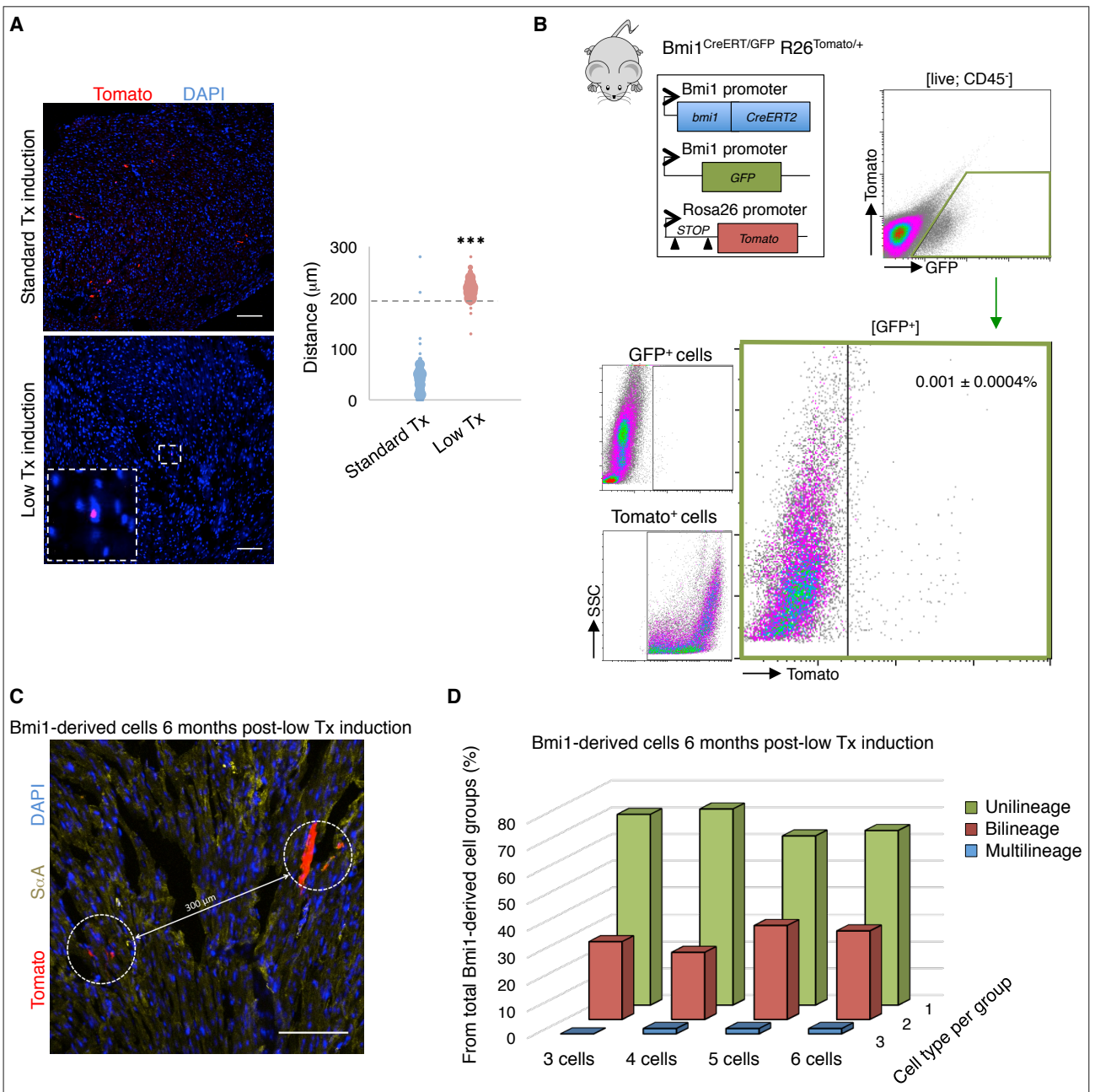


Figure III. Low-dose Tx labels mainly Bmi1⁺ cardiac cells with limited multilineage differentiation capacity. **A**, Representative heart cryosections (left) and quantification (right) of the distance between Bmi1⁺ progenitor cells after 5 days standard Tx (225 $\mu\text{g/g}$ body weight) compared to low-dose Tx induction (7.5 $\mu\text{g/g}$ body weight) in Bmi1^{CreERT/+}Rosa26^{Tomato/+} mice ($n = 3$). *Inset*, Bmi1⁺ cell (10x magnification). Bars, 100 μm . *** $p < 0.001$; two-sample Kolmogorov-Smirnov test. **B**, Representative FACS plot of Tomato⁺ cells in trigenic Bmi1^{CreERT/GFP}Rosa26^{Tomato/+} mice, 5 days post-low Tx induction ($n = 4$). **C**, Representative heart cryosection of two Bmi1-derived cell groups in Bmi1^{CreERT/+}Rosa26^{Tomato/+} mice, 6 months post-low Tx induction. Bar, 100 μm . **D**, Quantification of the multilineage identity of Bmi1-derived cell groups in Bmi1^{CreERT/+}Rosa26^{Tomato/+} heart cryosections, 6 months post-Tx low induction ($n = 3$). Data shown as mean \pm SEM.

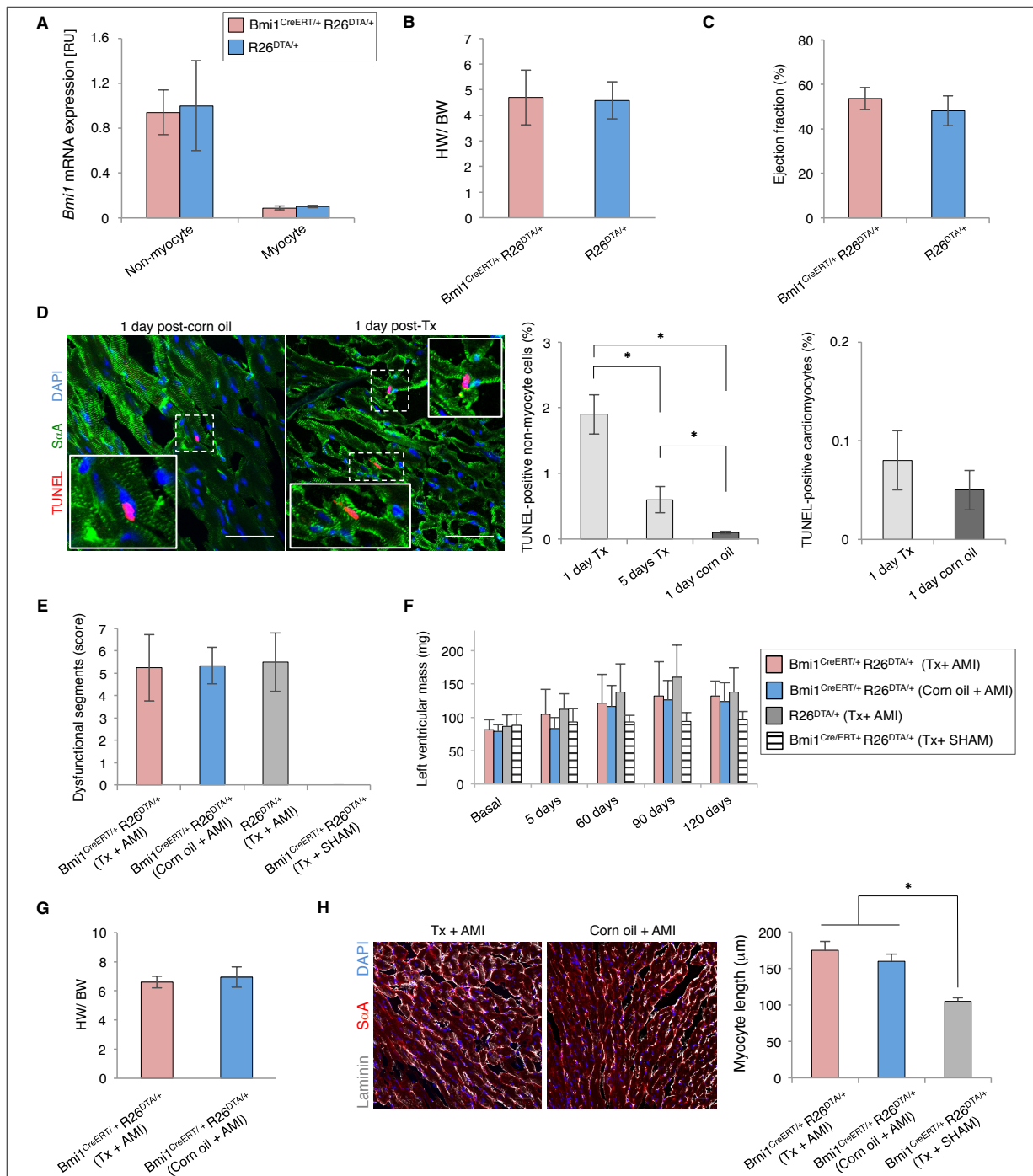


Figure IV. Bmi1^{CreERT/+}Rosa26^{DTA/+} hearts are normal and Tx activity induces non-myocyte Bmi1⁺ cardiac progenitor cell ablation. **A**, RT-qPCR analysis of *Bmi1* expression in non-myocyte and myocyte heart fractions from Bmi1^{CreERT/+}Rosa26^{DTA/+} mice compared to Rosa26^{DTA/+} age-matched controls in the absence of Tx ($n = 5$). n.s., not significant; Mann-Whitney rank sum test. **B** and **C**, Heart weight/body weight (HW/BW) ratio (**B**) and ejection fraction (**C**) of Bmi1^{CreERT/+}Rosa26^{DTA/+} adult hearts compared to Rosa26^{DTA/+} age-matched control hearts in the absence of Tx, measured by trans-thoracic M-mode echocardiography ($n = 5$). n.s.; Mann-Whitney rank sum test. **D**, Representative views (left) and quantification (right) of apoptosis in non-myocyte cells and cardiomyocytes from heart cryosections of vehicle- and Tx-induced Bmi1^{CreERT/+}Rosa26^{DTA/+} mice, 1 and 5 days after induction ($n = 3$). *Insets*, apoptotic cells (5x magnification). Bars, 100 μ m. * $p < 0.05$; Kruskal-Wallis ANOVA test. **E**, Trans-thoracic M-mode echocardiography showed no difference in the score of cardiac dysfunctional segments among the mouse groups studied; 5 days after AMI. n.s.; one-way ANOVA with Tukey's post-hoc test. **F**, LV mass measured by trans-thoracic M-mode echocardiography. n.s.; one-way ANOVA with Tukey's post-hoc test. **G**, HW/BW ratio of vehicle- (blue) and Tx-induced (red) Bmi1^{CreERT/+}Rosa26^{DTA/+} hearts, 4 months after AMI. n.s.; unpaired Student's t-test. (**E**, **F** and **G**: $n \geq 10$). **H**, Left: Representative cryosections showing cardiomyocyte size in Tx- and vehicle-treated Bmi1^{CreERT/+}Rosa26^{DTA/+} hearts, 4 months after AMI. Bars, 50 μ m. Right: Quantification of histological myocyte length for Tx- and vehicle-treated Bmi1^{CreERT/+}Rosa26^{DTA/+} compared to sham-operated age-matched control mice, 4 months after AMI ($n = 4$). * $p < 0.05$; Kruskal-Wallis ANOVA test. Data shown as mean \pm SEM.

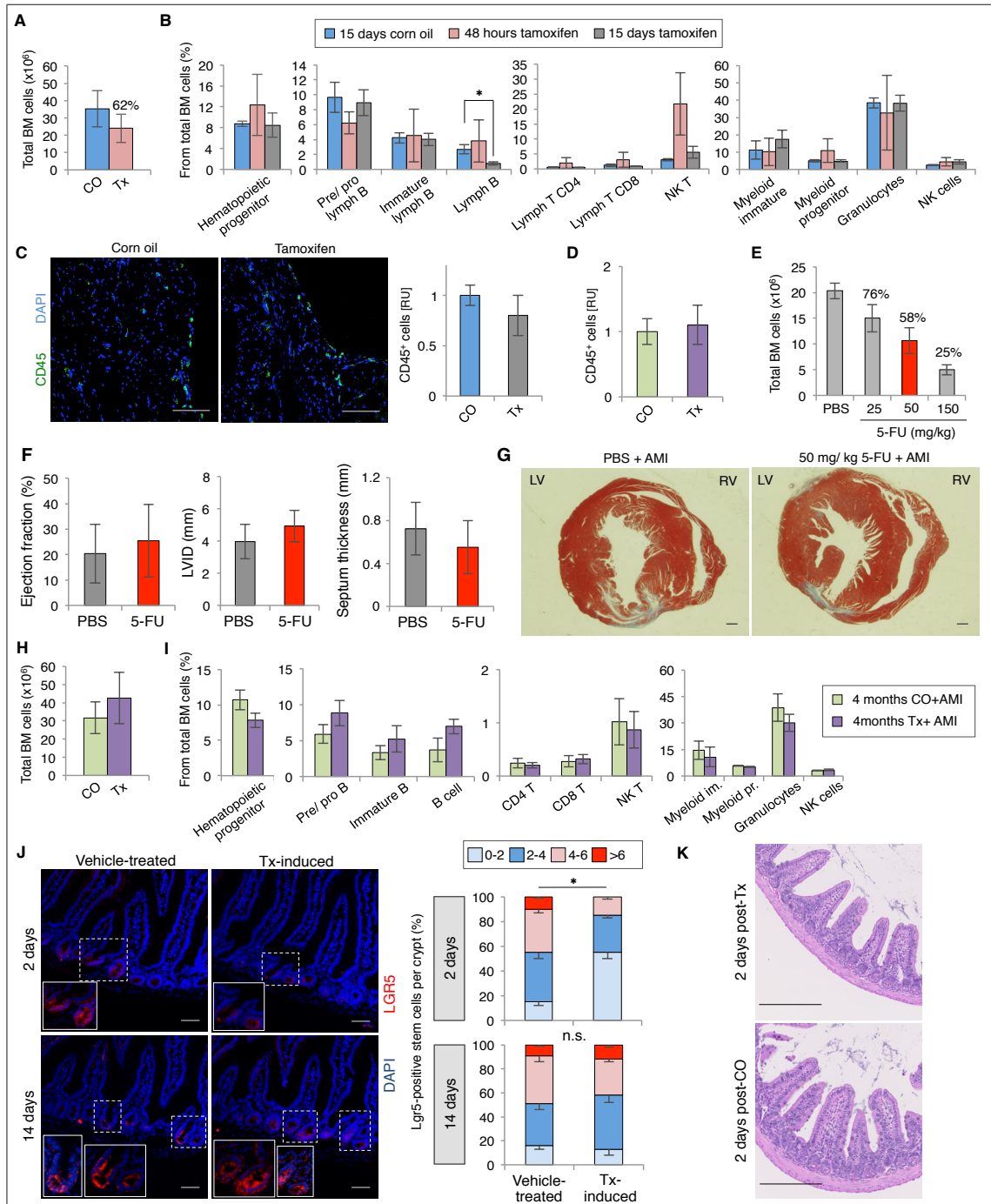


Figure V. Extra-cardiac *Bmi1*⁺ cell ablation. **A**, Quantification of BM cellularity in Tx-induced *Bmi1*^{CreERT/+}*Rosa26*^{DTA/+} femurs at 48 h (red) vs. vehicle-treated *Bmi1*^{CreERT/+}*Rosa26*^{DTA/+} mice (blue) (*n* = 3). n.s.; Mann-Whitney rank sum test. **B**, Analysis of BM cell populations in *Bmi1*^{CreERT/+}*Rosa26*^{DTA/+} mice at 48 h (red) and 15 days (grey) post-Tx induction compared to vehicle-treated *Bmi1*^{CreERT/+}*Rosa26*^{DTA/+} mice (blue) (*n* = 3). * *p* < 0.05; Kruskal-Wallis ANOVA test. **C** and **D**, Representative CD45 immunohistochemistry on heart cryosections (left) and quantification (right) of CD45⁺ cells in Tx-induced *Bmi1*^{CreERT/+}*Rosa26*^{DTA/+} (Tx) compared to vehicle-treated *Bmi1*^{CreERT/+}*Rosa26*^{DTA/+} hearts (CO), 15 days after induction (*n* = 3) (**C**) and 4 months after induction + AMI (**D**). Bars, 50 μ m. n.s.; Mann-Whitney rank sum test. **E**, Quantification of BM cellularity in femurs from 5-fluorouracil (5-FU)-treated *Bmi1*^{CreERT/+}*Rosa26*^{DTA/+} mice (*n* = 3). **F**, Trans-thoracic M-mode echocardiography and physiological parameters of 5-FU (50 mg/kg) (red) and vehicle-treated (grey) *Bmi1*^{CreERT/+}*Rosa26*^{DTA/+} mouse hearts, two months after AMI (*n* = 7). LVID: Left ventricular internal diameter. n.s.; Student's *t*-test. **G**, Representative transversal paraffin sections of Masson's trichrome staining to detect fibrosis and show anatomy of 5-FU (50 mg/kg) and vehicle-treated *Bmi1*^{CreERT/+}*Rosa26*^{DTA/+} mice, 4 months after AMI. Bars, 1 mm. **H** and **I**, Quantification of femur cellularity (**H**) and BM cell populations (**I**) in Tx-induced *Bmi1*^{CreERT/+}*Rosa26*^{DTA/+} mice (purple) compared to vehicle-treated *Bmi1*^{CreERT/+}*Rosa26*^{DTA/+} mice (green), 4 months after AMI (*n* = 3). n.s.; Kruskal-Wallis ANOVA test. **J**, Representative images (left) and quantification (right) of *Lgr5*⁺ intestinal cells at 2 and 15 days post-Tx induction compared to vehicle-treated *Bmi1*^{CreERT/+}*Rosa26*^{DTA/+} mice (*n* = 4). * *p* < 0.05; Kolmogorov-Smirnov test. Bar, 50 μ m. **K**, Representative Masson's trichrome-stained transverse paraffin sections to show the anatomy of Tx- and vehicle-treated *Bmi1*^{CreERT/+}*Rosa26*^{DTA/+} mouse intestine, 2 days post-induction. Bars, 250 μ m.

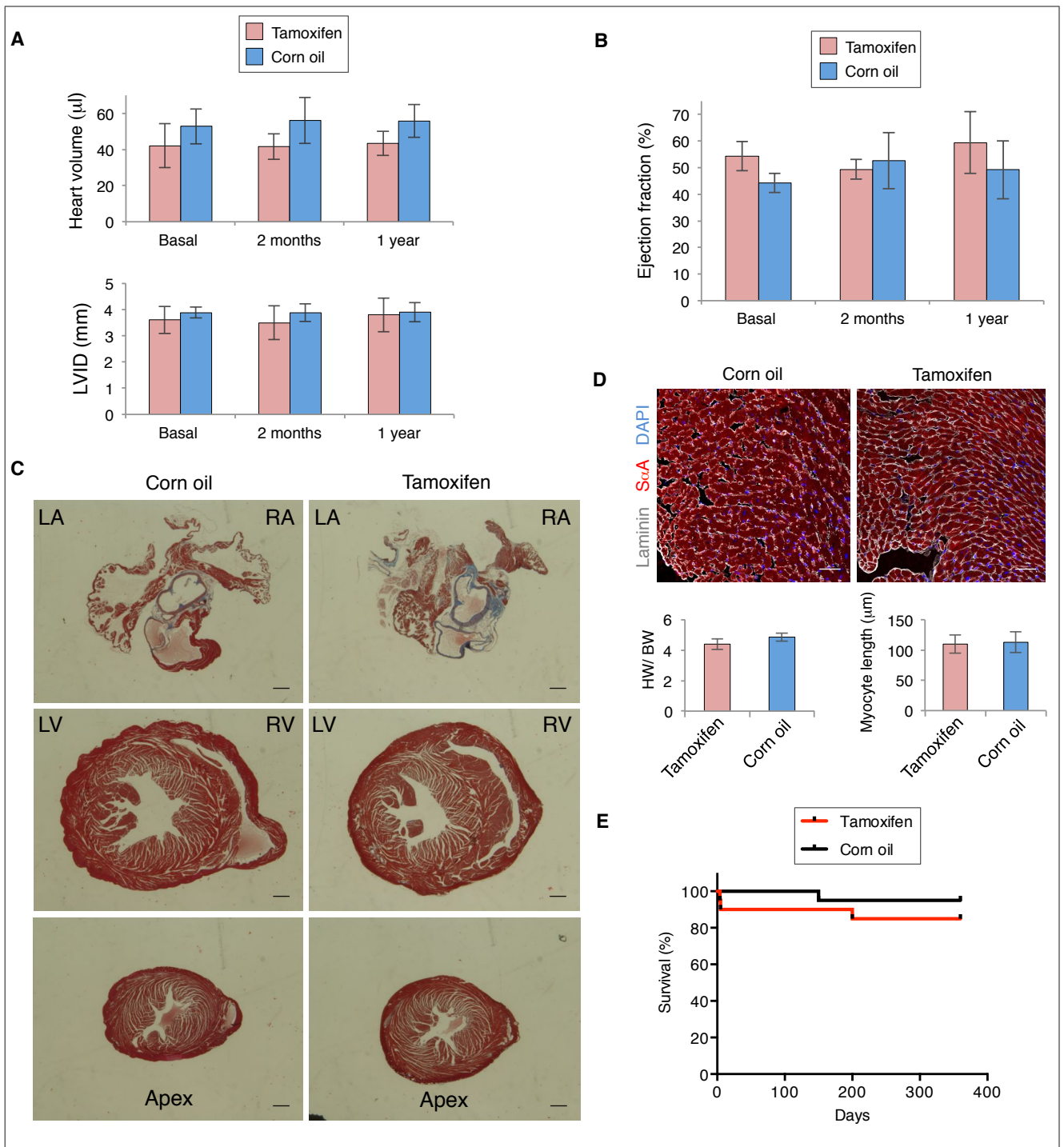


Figure VI. Bmi1-progenitor cell ablation does not affect heart function in homeostasis. **A** and **B**, Trans-thoracic M-mode echocardiography of physiological parameters (**A**) and ejection fraction (**B**) of Tx- and vehicle-treated (corn oil) Bmi1^{CreERT/+}Rosa26^{DTA/+} mouse hearts before (basal), 2 months, and 1 year after induction ($n = 5$). LVID: Left ventricular internal diameter. n.s., not significant; Kruskal-Wallis ANOVA test. **C**, Representative Masson's trichrome-stained transverse paraffin sections to detect fibrosis and show the anatomy of Tx- and vehicle-treated Bmi1^{CreERT/+}Rosa26^{DTA/+} mouse hearts, 1 year after induction. Bars, 1 mm. **D**, Top: Representative cryosections to show cardiomyocyte size in Tx- and vehicle-treated Bmi1^{CreERT/+}Rosa26^{DTA/+} mouse hearts, 1 year after induction. Bars, 50 μm. Bottom: Quantification of heart weight/body weight (HW/BW) ratio ($n = 5$) and histological myocyte length ($n = 3$) for Tx- and vehicle-treated Bmi1^{CreERT/+}Rosa26^{DTA/+} mice, 1 year after induction. n.s.; Mann-Whitney rank sum test. **E**, Kaplan-Meier survival curves for the indicated groups of Bmi1^{CreERT/+}Rosa26^{DTA/+} mice ($n = 30$). LV: left ventricle, RV: right ventricle, LA: left atrium, RA: right atrium. Data shown as mean \pm SEM.

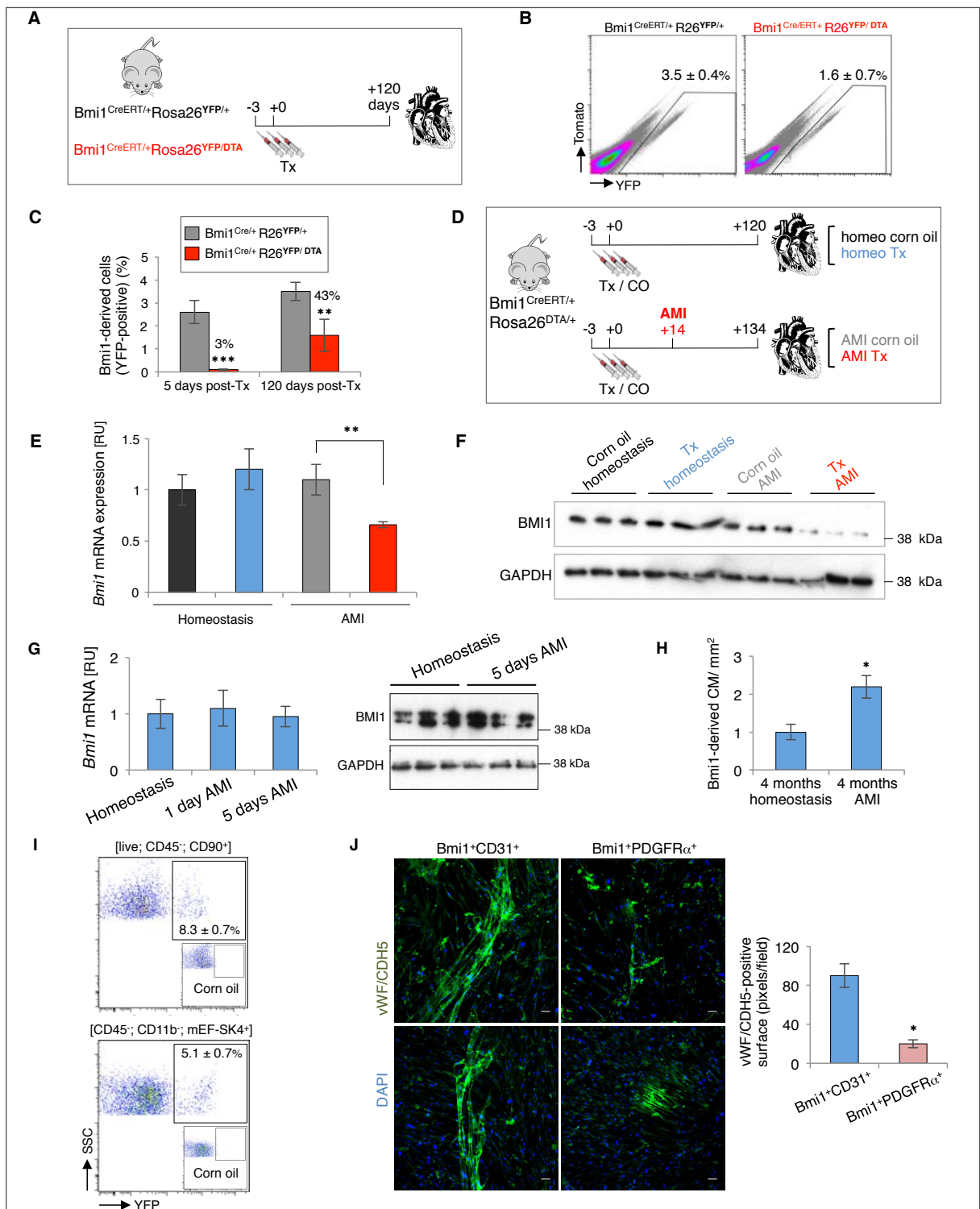


Figure VII. Cardiac cell plasticity. **A**, Timeline strategy of Bmi1-derived cell (YFP⁺) analysis in hearts from Bmi1^{CreERT/+}Rosa26^{YFP/+} vs. Bmi1^{CreERT/+}Rosa26^{YFP/DTA} mice. **B** and **C**, Comparative FACS plots (**B**) and quantification (**C**) of Bmi1-derived cells (YFP⁺) from bigenic Bmi1^{CreERT/+}Rosa26^{YFP/+} vs. trigenic Bmi1^{CreERT/+}Rosa26^{YFP/DTA} hearts, 5 days and 4 months post-Tx induction ($n \geq 6$). ** $p < 0.005$, *** $p < 0.001$; one-way ANOVA with Tukey's post-hoc test. **D**, Timeline strategy of BMI1 analysis in adult Bmi1^{CreERT/+}Rosa26^{DTA/+} hearts. **E** and **F**, Bmi1 expression in whole hearts from vehicle- and Tx-induced Bmi1^{CreERT/+}Rosa26^{DTA/+} mice, 4 months post-Tx induction (homeostasis) and 4 months after myocardial infarction (AMI), measured by RT-qPCR (**E**) and Western blot (**F**) ($n \geq 3$). ** $p < 0.005$; Mann-Whitney rank sum test. **G**, AMI did not induce Bmi1 upregulation, 1 or 5 days after damage, measured by RT-qPCR (left) and Western blot (right) in whole hearts of C57BL/6 mice ($n = 3$). n.s.; Kruskal Wallis ANOVA test. **H**, Quantification of Bmi1-derived cardiomyocytes in heart cryosections from Bmi1^{CreERT/+}Rosa26^{YFP/+} mice at four months after AMI compared to age-matched mice in homeostasis ($n = 3$). * $p < 0.05$; Mann-Whitney rank sum test. **I**, FACS plots of Bmi1-derived fibroblasts (YFP⁺CD90⁺/YFP⁺CD11b⁺mEF-SK4⁺) from non-myocyte heart fractions of Bmi1^{CreERT/+}Rosa26^{YFP/+} mice, 4 months after AMI ($n = 3$). **J**, *In vitro* spontaneous differentiation to endothelial cell lineage (left) and quantification (right) of Bmi1⁺CD31⁺ vs. Bmi1⁺PDGFR α ⁺ progenitor cells from Bmi1^{CreERT/+}Rosa26^{YFP/+} mice. ($n = 4$) Bar, 50 μ m. * $p < 0.05$; Mann-Whitney rank sum test. Data shown as mean \pm SEM.

Genotype	Description	Experiments
$Bmi1^{GFP/+}$	To identify <i>Bmi1</i> -positive cells based on green fluorescence protein (GFP) expression	<ul style="list-style-type: none"> - Characterization of <i>Bmi1</i> expression in adult heart - Isolation of <i>Bmi1</i>-positive cardiac cells
β -actin ^{GFP/+}	Control of constitutive GFP expression	<ul style="list-style-type: none"> - Constitutive GFP expression in adult cardiac cells (positive control)
$Bmi1^{CreERT/+}$ $Rosa26^{Tomato/+}$ $Bmi1^{CreERT/+}$ $Rosa26^{YFP/+}$	<p>At the time of tamoxifen induction, <i>Bmi1</i>-expressing cells activate the CRE enzyme, which induces the constitutive fluorochrome expression</p> <p>$Bmi1^{CreERT}$ allele does not modify endogenous expression of <i>Bmi1</i></p>	<ul style="list-style-type: none"> - Identification of <i>Bmi1</i>-positive cells in adult heart after tamoxifen induction - Isolation of <i>Bmi1</i>-positive cardiac cells - Tracking <i>Bmi1</i>-derived cells in adult heart
$Bmi1^{CreERT/+}$ $Rosa26^{DTA/+}$	At the time of tamoxifen induction, <i>Bmi1</i> -expressing cells activate CRE, which induces diphtheria toxin A expression	<ul style="list-style-type: none"> - Ablation of <i>Bmi1</i>-positive cells in adult mice, avoiding development-associated effects - Cardiac functional analyses
$Bmi1^{CreERT/+}$ $Rosa26^{YFP/DTA}$	At the time of tamoxifen induction, <i>Bmi1</i> -expressing cells activate CRE, which induces diphtheria toxin A expression and constitutive fluorochrome expression	<ul style="list-style-type: none"> - Analysis of DTA ablation efficiency of <i>Bmi1</i>⁺ cardiac progenitor cells after tamoxifen induction
$Bmi1^{GFP/CreERT}$ $Rosa26^{Tomato/+}$	<i>Bmi1</i> -positive cells express GFP and, after Tx induction, <i>Bmi1</i> -expressing cells activate CRE, which induces constitutive Tomato expression	<ul style="list-style-type: none"> - Analysis of the percentage of GFP⁺ cells (<i>Bmi1</i>⁺) labeled with Tomato after low-dose Tx induction

Table I. Transgenic mouse lines used in this study

Primary antibodies

Antigen	Application (Dilution)	Reference
CDH5	IHC-Fr, ICC (10 µg/ml)	MA5-17050 Thermo Fisher
vWF	IHC-Fr, ICC (10 µg/ml)	Ab11713 abcam
CD146	IHC-Fr (1 µg/ml)	Ab75769 abcam
ScA	IHC-Fr (10 µg/ml)	A7732 Sigma
αSMA	IHC-Fr (10 µg/ml)	A2547 Sigma
Laminin	IHC-Fr (1 µg/ml)	Ab11575 Sigma
YFP	IHC-Fr (10 µg/ml)	AB603 Evrogen
Collagen-1α	IHC-Fr (15 µg/ml)	1310-01 Southern Biotec
GFP	IHC-Fr (5 µg/ml)	632592 Clontech
SCA-1	IHC-Fr (1 µg/ml)	Ab25196 abcam
CD140a	IHC-Fr (5 µg/ml)	14-1401-82 Thermo Fisher
CD90	IHC-Fr (5 µg/ml)	105317 BioLegend
Nestin	IHC-Fr (10 µg/ml)	MAB353 Millipore
CD105	IHC-Fr (2 µg/ml)	12-1051-82 Thermo Fisher
FSP1	IHC-Fr (2 µg/ml)	A5114 Dako
LGR5	IHC-Fr (5 µg/ml)	Ab75850 Sigma
CD31	FACS (2 µg/ml)	553372 BD Pharmingen
CD140a-APC	FACS (4 µg/ml)	135907 BioLegend
CD90-biotin	FACS (2 µg/ml)	25-0902-82 BD Biosciences
mEF-SK4	FACS (3 µg/ml)	130-102-352 Miltenyi
CD45-eF450	FACS (2 µg/ml)	48-0451-82 eBioscience
CD34	FACS (10 µg/ml)	11-0341-85 eBioscience
IgM	FACS (5 µg/ml)	1020-02 B Coulter
B220	FACS (2 µg/ml)	103234 BioLegend
Gr1	FACS (5 µg/ml)	732488 B Coulter
CD4	FACS (2 µg/ml)	17-0042-83 eBioscience
CD8	FACS (2 µg/ml)	100732 BioLegend
TCRb	FACS (5 µg/ml)	732247 B Coulter
F4/80	FACS (5 µg/ml)	11-4801-85 eBioscience
CD11b	FACS (2 µg/ml)	733270 B Coulter
BMI1	WB (5 µg/ml)	05-647 Millipore
GAPDH	WB (1 µg/ml)	Ab9485 abcam

IHC-Fr: immunohistochemistry on frozen sections; ICC: immunocytochemistry;
WB: Western blot; FACS: flow cytometry

Primers

Gene	Sequence 5'-3'
<i>Bmi1</i>	Fw: CGCCCGCTCAGATCGCCTC Rv: ACCCTCCACACAGGACACACATT
<i>Tie2</i>	Fw: TTTGCGGATCAGACACAAGA Rv: CCGGCTTAGTTCTCTGTGGA
<i>cd31</i>	Fw: AGTTGCTGCCATTTCATCAC Rv: CCGAACGTCGTATCTCCTGGTC
<i>αSMA</i>	Fw: CTGACAGAGGCACCACAGTAA Rv: CATCTCCAGAGTCCAGCACA
<i>Collagen1a1</i>	Fw: TGAAGGAGAGCGGAGAGT Rv: GTTCGGGCTGATGTACCAGT
<i>s100a</i>	Fw: TTTGTGGGAGGCTGGACACAA Rv: CAGCACTTCTCTCTCTTGG
<i>Cdh5</i>	Fw: TCATCAAACCCACGAAAGTCC Rv: GGTCTGTGGCCTCAATGTAGA
<i>Vegfa</i>	Fw: AAGGAGAGGGCAGAATCAT Rv: ATCTGCATGGTGTGTTGGA
<i>Vwf</i>	Fw: CCGTCTTCAGTAGCTGGCAT Rv: GTGTAACGGGCATCTCCTC
<i>GusB</i>	Fw: ACTCCTCACTGAACATGCCGA Rv: ATAAGAGGCATCAGAAGCCG
<i>Gapdh</i>	Fw: AGGTCGGTGTGAACGGATTTG Rv: TGTAGACCATGTAGTTGAGGTCA
<i>cd34</i>	Fw: TGAAAAAGCTGGGGATCCT Rv: TCCCAGTCTCTGAGCTATA
<i>Kdr</i>	Fw: AGAACACAAAAGAGAGAGGAACG Rv: GCACACAGGCAGAAACAGTAG
<i>cd146</i>	Fw: AGGACCTTGAGTTTGAGTGG Rv: CAGTGGTTTGGCTGGAGT
<i>Ly6a</i>	Fw: GGCAGATGGGTAAGCAAAGA Rv: CAATTACCTGCCCTACCTT
<i>Nestin</i>	Fw: CCCTGAAGTCGAGGAGCTG Rv: CTGCTGCACCTCTAAGCGA
<i>humanBMI1</i>	Fw: CCGGCTGCTCTTTCCGGGATT Rv: CCCTCCACAAAGCACACATCAGG
<i>humanGADPH</i>	Fw: AACTGCTTGGCACCCCTGGC Rv: CTGGAGAGCCCTCGGCCAT

Table II. List of primary antibodies and RT-qPCR primers used in this study